Universiteit Antwerpen

This item is the archived peer-reviewed author-version of:

Foundations of modelling of nonequilibrium low-temperature plasmas

Reference:
Alves L.L., Bogaerts Annemie, Guerra V., Turner M.M..- Foundations of modelling of nonequilibrium low-temperature plasmas
Plasma sources science and technology / Institute of Physics [Londen] - ISSN 0963-0252 - Bristol, Iop publishing ltd, 27:2(2018), 023002
Full text (Publisher's DOI): https://doi.org/10.1088/1361-6595/AAA86D
To cite this reference: https://hdl.handle.net/10067/1493910151162165141

uantwerpen.be
Institutional repository IRUA

Foundations of modelling of nonequilibrium low-temperature plasmas

L. L. Alves[1], A. Bogaerts[2], V. Guerra[1], M. M. Turner[3]

[1] Instituto de Plasmas e Fusão Nuclear, Instituto Superior Técnico, Universidade de Lisboa, Av. Rovisco Pais, 1049-001 Lisboa, Portugal

[2] Department of Chemistry, Research Group PLASMANT, University of Antwerp, Universiteitsplein 1, B-2610 Antwerp, Belgium

[3] School of Physical Sciences and National Centre for Plasma Science and Technology, Dublin City University, Dublin 9, Ireland

E-mail: `llalves@tecnico.ulisboa.pt`

December 21, 2017

Abstract. This work explains the need for plasma models, introduces arguments for choosing the type of model that better fits the purpose of each study, and presents the basics of the most common nonequilibrium low-temperature plasma models and the information available form each one, along with an extensive list of references for complementary in-depth reading. The paper presents the following models, organized according to the level of multi-dimensional description of the plasma: kinetic models, based on either a statistical particle-in-cell / Monte-Carlo approach or the solution to the Boltzmann equation (in the latter case, special focus is given to the description of the electron kinetics); multi-fluid models, based on the solution to the hydrodynamic equations; global (spatially-average) models, based on the solution to the particle and energy rate-balance equations for the main plasma species, usually including a very complete reaction chemistry; mesoscopic models for plasma-surface interaction, adopting either a deterministic approach or a stochastic dynamical Monte-Carlo approach. For each plasma model, the paper puts forward the physics context, introduces the fundamental equations, presents advantages and limitations, also from a numerical perspective, and illustrates its application with some examples. Whenever pertinent, the interconnection between models is also discussed, in view of multi-scale hybrid approaches.

Keywords: low-temperature plasmas, modelling, particle-in-cell, kinetic equation, fluid model, global model, plasma-surface mesoscopic model

Submitted to: *Plasma Sources Sci. Technol.*

1. Introduction

The field of low-temperature plasma (LTP) science and engineering has been driven by both fundamental science issues and applications targeting societal benefits [1]. Fundamental research strives to gain deeper understanding of the underlying principles governing these plasmas, and is essential to ensure the scientific advances required for consolidated successful applications.

Modelling activities are a fundamental component of any research field, to complement and/or assist the implementation of experimental diagnostics; to give predictions on the behaviour of meaningful quantities, especially when these are inaccessible experimentally; and to deepen fundamental knowledge of the field. The modelling and simulation of LTPs has been considered a requirement for the progress in the field [1,2], and model-based design for plasma equipment and processes has been identified as a necessary capability to achieve industrial goals [3]. Indeed, the guidance provided by LTP models is particularly relevant due to the extreme complexity of the medium (often exhibiting different material phases), composed by charged particles (electrons and ions) and by neutral species in different excited states, intrinsically in non-equilibrium as result of collisional, radiative and electromagnetic interactions.

The success in the modelling and simulation of LTPs is impressive, given the extreme diversity of the field, including types of plasma sources, pressures, spatial and time scales, electron energies and chemistries. This diversity can only be met by a suite of models, adopting formulations and algorithms adapted to the specific working conditions and features of each gas/plasma system. This work integrates the collection of papers published by Plasma Sources Science and Technology on Foundations of Low-Temperature Plasmas and Their Applications, conveying essential information to enable a beginner in this field to identify the most common nonequilibrium LTP models and the information available from each one. Models of plasmas in local thermodynamic equilibrium are addressed in a different paper of the same collection [4], on the "Foundations of high-pressure thermal plasmas". For each plasma model, this paper puts forward the physics context, introduces the fundamental equations, presents advantages and limitations, also from a numerical perspective, and gives some illustrative examples. Only key information is given, to make clear the type of model that best suits the purpose of each study, in addition to an extensive list of references for complementary in-depth reading.

The organisation of this paper is the following. Sections 2 and 3 introduce kinetic models, based on a statistical particle-in-cell / Monte-Carlo approach or the solution to the Boltzmann equation, with special focus on the description of the electron kinetics. Section 4 is dedicated to fluid models, based on the solution to the hydrodynamic equations for the multi-fluid system of electrons, ions and neutrals that compose plasma. Section 5 presents global (spatially-averaged) models, based on the solution to the particle and energy rate-balance equations for the main plasma species, usually including a comprehensive reaction chemistry. Section 6 introduce mesoscopic models for

plasma-surface interaction, which adopt either a deterministic approach or a stochastic dynamical Monte-Carlo approach. Section 7 concludes with final remarks.

The text of the paper uses various acronyms and introduces many physical quantities, which are not always defined when they appear for the first time in the equations. Tables 1-3 present the list of symbols, the list of physical constants and the list of acronyms, respectively, as used in the paper.

2. Plasma particle-in-cell simulation

A LTP is a mixture of charged and neutral particles. In a general way, each of these species can be characterized by a particle distribution function, which depends on both velocity space and real space coordinates. If there is also time dependence, then in the most general case there are seven independent variables. In a nonequilibrium LTP, there is no thermalization between the populations of the different species, each having a particle distribution function with a different mean energy. The evolution of the particle distribution functions is described by a Boltzmann transport equation for each species [5] (see section 3), and these equations are coupled to each other through collisional interactions. If this were not already a sufficiently complex problem, charged species additionally interact with electromagnetic fields, which may be either self-generated or externally applied. If these fields are to be consistent with the particle distribution functions, then the set of Boltzmann equations must be coupled to Maxwell's equations. The solution of this system of equations is a challenge almost always beyond the resources available to LTP physicists, so that simplifications must usually be sought. Most methodologies for generating numerical solutions of systems of partial differential equations replace the continuous functions of the mathematical problem with a finite set of values, typically specified at a set of points defined by dividing each coordinate axis into uniform intervals. If there are N_I such intervals on each axis, and the problem has d dimensions, then the number of values to be computed is $(N_I)^d$. If $N_I = 100$ (a modest number), then a single seven dimensional particle distribution function involves the computation of some 10^{14} values, which shows why such calculations are not much attempted. Clearly, the most direct way to manage this formidable number is to reduce the number of dimensions. Reducing the number of real space dimensions simplifies the physical problem rapidly and drastically, but whether or not this is acceptable depends on the objectives of the computation. Reducing the number of velocity space dimensions is equally powerful, but has more subtle physical consequences. An elegant approach that is discussed in detail in section 3 of this article expresses the particle distribution function in velocity space (also called the velocity distribution function) in terms of a spherical harmonic expansion. This method reduces the number of velocity space coordinates from three to one (and, therefore, reduces the computational burden by a factor $\sim 10^4$), often without much loss of physical fidelity, at least where electrons are concerned. However, in principle, the spherical harmonic approximation does not work well for ions, and may not be satisfactory for

electrons in regions of strong electromagnetic fields. In practice, the spherical harmonic approximation is frequently combined with further approximations affecting the coupling between charged particles and fields. For these reasons, numerical schemes that compute the particle distribution functions without such simplifying assumptions are of interest. In this context, we introduce particle-in-cell simulation.

Particle-in-cell (PIC) simulation adopts a different strategy for reducing the amount of computation [6–8]. Instead of spanning each velocity axis with fixed points where the values of the particle distribution functions are computed, a PIC simulation introduces a set of particles that move through velocity and real space under the action of electromagnetic fields. The physical particle distribution function is then expressed as a sum over the set of computational particles. A high degree of accuracy can be achieved with a surprisingly small number of particles. The real space axes are divided into intervals as before, so that one can speak of real space as divided into *cells*, and every particle is therefore located in such a cell, hence the name of the method. Many calculations can be satisfactorily accomplished with around 100 particles per cell, so the reduction in computational burden is again around 10^4, which seems similar to a spherical harmonic expansion. However, for reasons of stability and accuracy, the cell sizes in PIC simulations are restricted by basic plasma properties such as the plasma frequency and the Debye length. A simulation method based on a spherical harmonic expansion usually adopts additional assumptions that avoid these constraints, so that in practice a PIC simulation is appreciably more costly — probably by at least a factor of ten in most cases, and sometimes much more.

2.1. Basic approach

This section will display the basic characteristics of the PIC method by discussing the simplest case of a system with three dimensions — one real space, one velocity space and time. The equations of motion for the charged particles can include relativistic or quantum effects in a semi-classical approximation [7], but these are usually not needed in LTPs, so the relevant formulation is:

$$\frac{dx_i}{dt} = v_i \tag{1}$$

$$\frac{dv_i}{dt} = \frac{q_\alpha}{m_\alpha} E(x_i) \quad , \tag{2}$$

where here the index i refers to a particle and α a species (electrons or ions). Of course, all particles of the same species have the same mass m_α and charge q_α. This formulation (and the discussion below) refers to the simplest case where only one axis is considered in both real and velocity space. More general formulations, including magnetic field effects, are basically similar in structure, and can be found in the literature [6, 7]. In the electrostatic case, the electric field $E(x) = -d\Phi(x)/dx$ (with $\Phi(x)$ the electrostatic potential) is found by solving the Poisson equation

$$\frac{d^2\Phi}{dx^2} = -\frac{\rho}{\epsilon_0} \quad , \tag{3}$$

where the charge density ρ is found by summing contributions from particle species:

$$\rho = \sum_\alpha \rho_\alpha \quad . \tag{4}$$

We divide the x axis into a finite set of cells by introducing a cell size Δx so that cell boundaries are at $x_k = k\Delta x$ with integral k. Then we replace the continuous Poisson equation with the discrete form:

$$\frac{\Phi_{k+1} - 2\Phi_k + \Phi_{k-1}}{\Delta x^2} = -\frac{\rho_k}{\epsilon_0} \quad , \tag{5}$$

where $\Phi_k = \Phi(x_k)$, *etc.* The charge densities ρ_α are expressed in terms of the particle coordinates by introducing a shape factor $S(x_k, x_i)$, such that

$$\rho_k = \sum_\alpha q_\alpha W_\alpha \sum_i S(x_k, x_i) \quad , \tag{6}$$

where W_α is a weight factor expressing the relationship between the density of computational particles and the physical density of the plasma. Each computational *macroparticle* represents many physical particles, of course. Many detailed properties of the algorithm depend on the shape factor, which may be variously chosen [6, 7]. In contemporary practice, the most common option is bi-linear weighting, which divides the charge of each particle between the two nearest grid points:

$$S(x_k, x_i) = \begin{cases} \frac{x_i - x_k}{\Delta x} & \text{if} \quad x_k \le x_i \le x_k + \Delta x \\ 0 & \text{otherwise} \end{cases} \quad . \tag{7}$$

This expression is generally [6, 7] perceived to give a good compromise between computational complexity and desirable algorithmic properties (which are elaborated below). The algorithm is completed by specifying a procedure for advancing the particle positions and velocities in time. Again, there are various options, but the most common choice is the so-called leap-frog method:

$$v_{i,n+\frac{1}{2}} = v_{i,n-\frac{1}{2}} + \frac{q_\alpha}{m_\alpha} E(x_i) \tag{8}$$

$$x_{i,n+1} = x_{i,n} + v_{i,n+\frac{1}{2}} \quad , \tag{9}$$

where n denotes the time level.

This method is a so-called *momentum conserving* algorithm: momentum conservation is an exact property of the equations [6, 7]. Energy, on the contrary, is conserved to an extent that depends on the numerical parameters, and, of course, a more conservative choice of these parameters will lead to improved energy conservation, as we will see below. There are variant PIC algorithms that work the other way around — these *energy conserving* methods have never been widely used, although they continue to attract interest, and they will not be discussed in detail here.

The procedure described above does not yet include collisional effects, and consequently is a method for solving the Vlasov equation (see section 3). An important property of the Vlasov equation is that for any plasma with spatial uniformity, such that electric fields are absent, any normalizable function of velocity is a stationary solution.

The PIC method does not exactly preserve this property. When the number of particles is finite, there is a graininess in the simulation that produces small electric fields, which fluctuate essentially randomly. These fluctuating fields cause the velocity distribution function to change in time — the velocity distribution evolves towards a Maxwellian, and there is a slow heating effect. These unphysical effects are measured by the collision time τ_C and the heating time τ_H [6, 7]. An aim of algorithmic design is to make these times as large as possible with the least computational effort. Optimising the shape factor is one of the most important of the available tools in this respect. Considerations of maximising τ_C and τ_H lead to the well-known and widely used accuracy conditions

$$\omega_P \Delta t \lesssim 0.2 \tag{10}$$

$$\frac{\lambda_D}{\Delta x} \gtrsim 2 \quad , \tag{11}$$

which connect the numerical parameters Δt and Δx with the basic time and length scales of the plasma, defined by the plasma frequency ω_p and the Debye length λ_D.

A real plasma also has a finite collision time, because the density of particles is actually finite, and this finiteness is usually measured by the number of particles in a Debye sphere. This number is typically around $O(10^4)$ for a LTP. For a three dimensional PIC simulation, this number may be compared with the number of particles per cell, which is $O(10^2)$. Hence one expects that collisional effects will be much more important in a PIC simulation than in a real plasma. However, these collisional effects are caused by electric field fluctuations with high frequencies and short wavelengths. The finite time step and cell size of the simulation act as filters for these high frequency field components, with the result that collisional effects are strongly attenuated. These factors combine to make PIC simulation a highly efficient method for solving the Vlasov equation, relative to alternative numerical procedures.

The limitations imposed by the requirement to resolve the Debye length and the plasma frequency are often serious. Attention has therefore been given to more complex approaches that avoid such constraints. These are *implicit* methods [6]. In the context of LTP physics, a basic difficulty with this approach is that there are interesting physical phenomena, often important, that involve these length and time scales (sheaths, for instance [9]). The computational advantages promised by an implicit approach are difficult to realise in a simulation that properly captures (for example) sheath phenomena, and so implicit methods have not been much used.

2.2. Collisions

The PIC method just described is an approach to solving the Vlasov equation, which includes no collisional effects. As we have seen, the collisional effects that occur in PIC simulations are numerical artifacts that are to be minimised by careful algorithmic design and proper selection of numerical parameters. Physical collisions, however, are essential to the behaviour of LTP. The customary method for including physical collisions in a PIC simulation is via a Monte Carlo (MC) procedure [8, 10, 11]. The simplest method

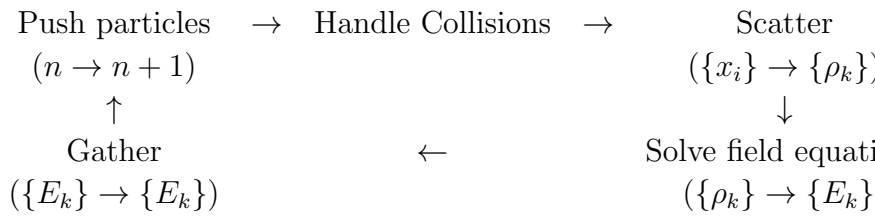

Figure 1. The computational cycle for a PIC simulation with MC collisions, showing how data is scattered from particles (labelled by index i) to mesh points (labelled by index k) in order to determine the fields at the mesh points. Then field data is gathered to the particle positions to effect an advance of time level from n to $n+1$.

(appropriate when the plasma frequency is large compared to the collision frequency, ν_c) is to assume that collisions occur only at the end of a simulation time step with a probability per particle given by

$$P = 1 - \exp(-\nu_c \Delta t) \approx \nu_c \Delta t \quad . \tag{12}$$

This expression involves the convenient assumption that ν_c does not depend on the particle velocity. In practice, ν_c has contributions from a number of physical processes, with varied dependences on the relative velocity of the colliding particles. An ingenious device for suppressing the velocity dependence of P is to include a so-called *null collision* process [12], such that for each particle species

$$\nu_c = \nu_{\rm null}(v) + \sum_i \nu_i(v), \tag{13}$$

where $\nu_i(v)$ is the velocity-dependent collision frequency of the $i^{\rm th}$ collision process, and $\nu_{\rm null}$ is chosen so that ν_c is in fact a constant. In this method, a second MC step is needed to select a collision process. If a real process is selected, then appropriate changes to the velocity of the colliding particle are made, but if the null collision is chosen, no such changes occur. The detail of collision handling can become complex, and will not be discussed in detail here. However, any collision process with physical relevance can be included, including collisions between particles, often using techniques derived from the simulation of low-density gas flows [13]. The computational cycle that results is shown in figure 1.

This discussion assumes that only collisions between plasma particles and a background gas are to be considered. When processes involving collisions between particles are important, a more elaborate approach to collision handling is needed. A usual assumption in this case is that particles residing in the same cell are eligible to collide with each other. Procedures for identifying candidate collision pairs and selecting collision processes using Monte Carlo methods are then similar to those used in the low density gas flow simulation method called Direct Simulation Monte Carlo (DSMC) [13]. This method is entirely compatible with PIC simulation, although careful choice of data structures may be required if the implementation is to be efficient.

A difficulty appears in handling collisions when species with very different physical densities are involved, as is frequently the case for electronegative discharges when the

electron density is much less than the ion density, or when the need arises to treat neutral species on the same footing as charged species. In such cases, the natural solution is to assign different weight factors W to species with different physical densities. This solution, however, introduces problems such as enforcing conservation laws in collisions between particles of different weights, creating and destroying fractions of particles, and possibly degradation of the numerical properties of the algorithm [13, 14]. We will not discuss the various solutions that have been proposed, beyond noting that none is fully satisfactory. Probably, uniform particle weights are the best solution, unless the computational consequences are really intolerable.

2.3. Computational cycle

The method known as particle-in-cell with Monte-Carlo collisions (PIC-MCC, or less often PIC-MC) is constructed by combining the methods described above into a single computational cycle that is repetitively applied to advance both particle coordinates and fields through a desired sequence of time levels. A common situation in LTP physics is that a quasi-stationary state of the physical system is sought, and this usually can be found only by a lengthy and expensive time integration. No widely accepted method has yet been found for accelerating this process, other than applying techniques of high performance computation. The relatively simple algorithms and data structures involved mean that such an approach is often highly effective, and may lead to accelerations by factors like ten or a hundred using moderately priced hardware. Improvements of this magnitude are generally harder to achieve by applying similar techniques to models with more complex structure (such as hybrid models). Consequently, a count of arithmetical operations may not adequately characterize the computation time needed to solve a PIC-MCC model relative to other kinds of model. Presumably for these reasons, PIC simulations have occasionally been found to be faster than fluid models [15] (see section 4), but this is no doubt an unusual occurrence.

2.4. Applications

PIC simulation is most often used when complex velocity distributions appear, and when these distributions are suspected to be tightly coupled to the detailed evolution of the fields in time and space. There are many examples in LTP physics where such conditions occur, including radio-frequency discharges [16], direct-current discharges [11] and ion-thrusters [17], to mention only three cases. An early instance appears as figure 2, which depicts electron energy distribution functions (see section 3) in a radio-frequency discharge in nitrogen, showing how PIC simulation captures the complex structure of the distribution functions together with the changes that occur under different conditions.

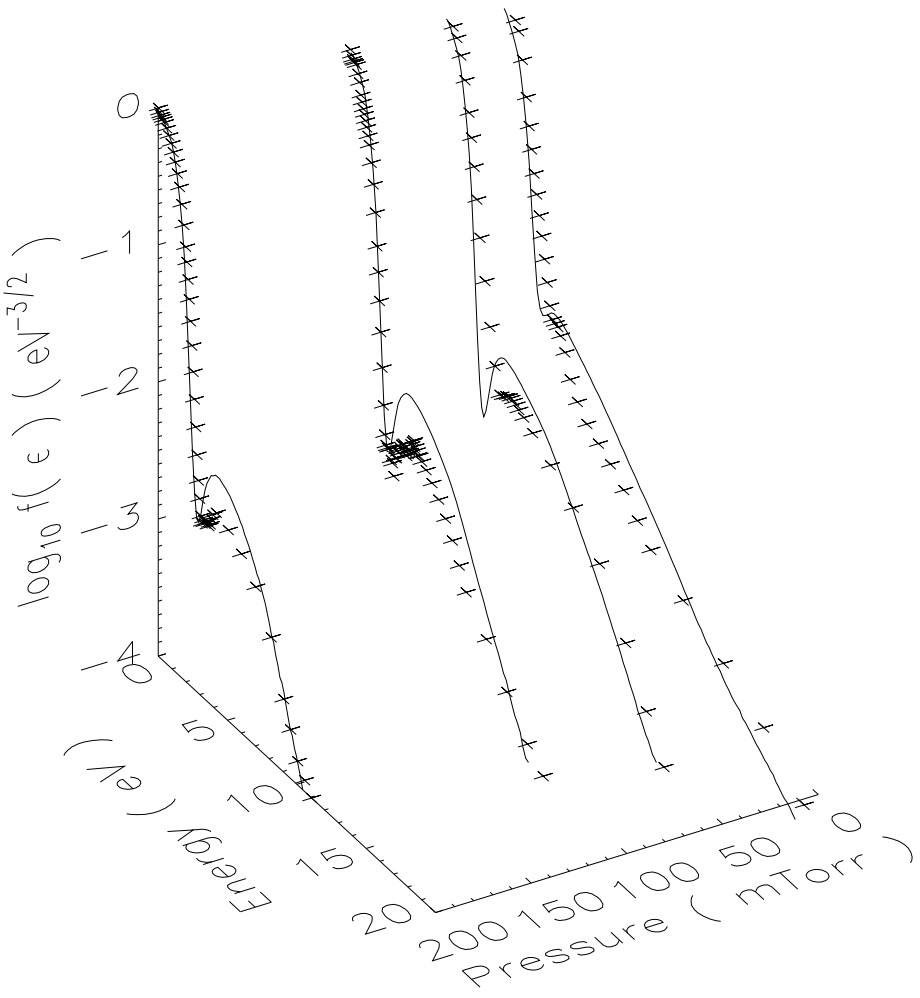

Figure 2. Electron energy distribution functions in a radio-frequency discharge in nitrogen, measured using a Langmuir probe (points) and computed from a PIC-MCC simulation (lines). This result shows the capacity of the PIC method for computing complicated energy distributions in good agreement with experiment (from [16]).

2.5. Areas of active research

In general, the PIC method is a mature technique. There has not, for example, been any dramatic change in the essential approach over the last two or three decades. However, research and development continues. For instance, the preferred data structure and detailed implementation have evolved over time in response to changes in the predominant computer architecture, such as from vector machines to distributed memory architectures, and most recently a combination of these techniques [18]. Some of the algorithmic limitations mentioned above (implicit methods, variable particle weights) continue to attract attention, and better solutions may be found. Particularly when two or three space dimensions are involved, techniques for dealing

with complex geometries are a matter of research [19]. In common with other areas of computational science, there is interest in the problem of demonstrating code correctness (*verification*) [15, 20, 21].

2.6. Summary

The PIC method is a simple and elegant approach to solving the Boltzmann equation without restrictive assumptions about the structure of the velocity distribution function or the coupling of the particle motions with the fields. As expected, the method keeps the limitations associated with solving this equation, such as the need for a discrete calculation of the fields and the assumption of binary collisions in the PIC-MCC formulation (on the latter issue, cf. section 3) for more details). For practical purposes, this approach gives the most accurate computational description of a LTP that is presently available. The rather simple character of the algorithm both conceals a high degree of theoretical sophistication and permits efficient implementations on modern high performance computers. Of course, there are many cases where special assumptions are applicable, and allow computationally less intensive methods to yield highly accurate results. But PIC remains a vital tool where no such assumptions have been discovered — which is often the case at the forefront of research.

3. Plasma kinetic equation models

The previous section showed that the kinetic description of weakly ionized gases can directly monitor the evolution of particles in phase space ($\vec{r}$, $\vec{v}$) and in time t, under the action of applied forces and due to collisions. An alternative approach for this analysis adopts the solution of a differential kinetic equation, to calculate the distribution of particles when subjected to similar phenomena in phase space and in time. The study is particularly important for the charged particles in a plasma, considering their key role in the non-local distribution of energy within the medium, and it applies to a dilute system of electrons and ions ($\alpha = e, i$), as usually considered in the classical kinetic theory of gases [22–24], with sufficiently high-temperature ($k_B T_\alpha \simeq 1$ eV) and low-density ($n_\alpha^{-1/3} \ll \lambda_D$ or $n_\alpha \ll \varepsilon_0 k_B T_\alpha / e^2 \simeq 1.7 \times 10^{23}$ m^{-3}). Under these conditions, each particle of the system has a classical behaviour, with well-defined position and momentum, and the dominant interactions are of short-range type, namely electron-molecule and ion-molecule collisions described using scattering cross sections. Plasma kinetic models rely essentially in the solution to the Boltzmann equation [24], whose collisional term is derived assuming (i) binary collisions, valid for a dilute system; (ii) interactions described by short-range weak central forces, whose effects are felt inside an elementary volume in position space, with negligible influence upon the collision cross section; (iii) molecular chaos, i.e. no correlations between the particles velocities for distances larger than the radial size of the collision volume, and no correlations between the velocities and the positions of the particles.

The analysis is based on the particle distribution function $F_\alpha(\vec{r}, \vec{v}_\alpha, t)$, defined so that $F_\alpha d\vec{r} d\vec{v}_\alpha$ represents the number of particles with positions in the interval $[\vec{r}, \vec{r} + d\vec{r}]$ and velocities in the interval $[\vec{v}_\alpha, \vec{v}_\alpha + d\vec{v}_\alpha]$, at time t. The volume elements $d\vec{r}$ and $d\vec{v}_\alpha$ are assumed big enough to contain a very large number of molecules, but small enough as compared to the dimensions of the system and to allow for the definition of meaningful local values for the position and the momentum of the particles. For a system with N_α particles, the normalisation of the particle distribution function is as follows

$$\int_{\vec{r}} \int_{\vec{v}_\alpha} F_\alpha(\vec{r}, \vec{v}_\alpha, t)\, d\vec{r} d\vec{v}_\alpha = N_\alpha(t) \quad , \tag{14}$$

and the corresponding particle number density n_α is defined as $\int_{\vec{v}_\alpha} F_\alpha(\vec{r}, \vec{v}_\alpha, t)\, d\vec{v}_\alpha = n_\alpha(\vec{r}, t)$.

3.1. Boltzmann equation for charged particles

The distribution of electrons and ions in a weakly ionized plasma satisfies the Boltzmann kinetic equation

$$\frac{\partial F_\alpha}{\partial t} + \vec{v}_\alpha \cdot \frac{\partial F_\alpha}{\partial \vec{r}} + \frac{\vec{X}_\alpha}{m_\alpha} \cdot \frac{\partial F_\alpha}{\partial \vec{v}_\alpha} = \left(\frac{\partial F_\alpha}{\partial t} \right)_{\text{coll}} \quad , \tag{15}$$

where $\partial/\partial\vec{r}$ and $\partial/\partial\vec{v}_\alpha$ represent the gradient operators in configuration space and in velocity space, respectively; $\vec{X}_\alpha/m_\alpha$ is the particle acceleration; and $(\partial F_\alpha/\partial t)_{\text{coll}} \equiv (\partial F_\alpha/\partial t)_{\alpha-\text{o}} + (\partial F_\alpha/\partial t)_{\text{charged}}$ is the rate of change of F_α due to electron-neutral collisions (e-o), ion-neutral collisions (i-o) and charged particle interactions (charged). The meaning of the Boltzmann equation becomes clear if one notes that the left-hand side of (15) represents the total (convective) derivative of F_α in phase space, dF_α/dt. Accordingly, the Boltzmann equation describes the rate of change of F_α as seen in a frame moving with the particles in the six-dimensional $(\vec{r}, \vec{v}_\alpha)$ space (left-hand side) and due to collisions (right-hand side). In the absence of collisions $dF_\alpha/dt = 0$, and when this result is articulated with the normalisation condition (14) it yields the conservation of the element volume $d\vec{r} d\vec{v}_\alpha$ (at constant particle number). In the presence of collisions, particles can be moved from one element of the phase space into another, and they can also be created / destroyed following non-conservative collisional mechanisms, such as ionisation / recombination and attachment / detachment.

Strictly, the Boltzmann equation cannot be used to describe the interactions between charged species, but only non-Coulomb interactions, such as electron-neutral and ion-neutral collisions [24, 25]. The reason is that charged-particle collisions are usually long-range correlated interactions, not accounted for in weakly ionized classical kinetic plasmas. Indeed, these plasmas are characterized by (i) short-range Coulomb interactions, which vanish for distances larger than the Debye length defined by the screen effect between oppositely charged particles; (ii) binary collisions with no correlations. The presence / absence of correlations within collisional encounters relates to the famous controversy around the removal / introduction of molecular

chaos when using the Boltzmann equation, and the reader should refer to other works (*e.g.* [23,24,26]) for more information. In moderately ionized plasmas, one can no longer disregard long-range Coulomb interactions due to the larger value of the charged-particle density. However, it is still possible to describe the interactions within the Debye sphere as a succession of continuous uncorrelated collisions, each producing a small deviation of the charged particles in phase space.

If only charged-particle interactions are considered, with no correlations, the collisional term can be written as [24, 26] $\left(\partial F_\alpha/\partial t\right)_{\text{charged}} = -\left(\partial F_\alpha/\partial \vec{v}_\alpha\right) \cdot \left(\vec{X'}_\alpha/m_\alpha\right)$, with $\vec{X'}_\alpha$ the space-charge interaction force, and the Boltzmann equation (15) becomes

$$\frac{\partial F_\alpha}{\partial t} + \vec{v}_\alpha \cdot \frac{\partial F_\alpha}{\partial \vec{r}} + \frac{\vec{X}_\alpha + \vec{X'}_\alpha}{m_\alpha} \cdot \frac{\partial F_\alpha}{\partial \vec{v}_\alpha} = 0 \quad . \tag{16}$$

Equation (16) is the so-called Vlasov equation, a collisionless kinetic equation accounting for the action of both the external forces applied to the charged particles and the space-charge forces resulting from Coulomb interactions.

If the Coulomb interactions are taken as binary collisions, causing small deflections in the charge-particle velocities, one obtains the Fokker-Planck equation [25, 27] (in the absence of spatial inhomogeneities)

$$\frac{\partial F_\alpha}{\partial t} + \frac{\partial}{\partial \vec{v}_\alpha} \cdot \left[\vec{\gamma}_\alpha F_\alpha - \frac{1}{2}\frac{\partial}{\partial \vec{v}_\alpha} \cdot \vec{\vec{\delta}}_\alpha F_\alpha\right] = 0 \quad , \tag{17}$$

where $\vec{\gamma}_\alpha$ and $\vec{\vec{\delta}}_\alpha$ are the α-particle dynamical-friction acceleration vector and the diffusion-in-velocity-space tensor, respectively, which depend on the distribution function of the target particles, the Rutherford cross section, and the velocities of the incident and the target particles.

The next subsections focus on the Boltzmann equation for electrons. The extreme diversity of LTPs pushes computer models to meet challenging requirements, simultaneously addressing fundamental plasma phenomena, so that a priori assumptions do not prejudice the result, while covering a wide variety of plasma equipment using different excitation schemes and complex volume and surface chemistries [28]. The details of this scenario are mostly promoted and defined by the electrons, the primarily species conveying energy to the plasma. Indeed, they are responsible for the selection of the main reactional mechanisms (excitation/deexcitation, dissociation, ionisation, recombination), conditioned by different electron populations with different energies. The description of non-equilibrium LTPs must therefore involve the calculation of the particle distribution function for electrons, for example by solving the corresponding Boltzmann equation, hence the choice for the topics of the next subsections. Note that other plasma components (ions, neutrals) may not require the same level of detail in their description, namely in what concerns the calculation of their velocity distribution functions that most often corresponds to an equilibrium Maxwellian distribution. The situation sets the basic premises of the so-called hybrid models [28], which use flexible and mixed calculation modules (among which an electron Boltzmann solver) adapted to the variety of species, physical phenomena and multi-time scales at hand.

3.2. Electron Boltzmann equation

The solution to the full Boltzmann kinetic equation (15) is a formidable problem mainly due to its multi-dimensionality and non-linearity. Apart from the inherent difficulties of working in a 7-dimensional space, the need for a self-consistent solution introduces additional complications associated with the appearance of crossed $(\vec{r}, \vec{v})$ derivatives, *e.g.* when dealing with the presence of electrostatic space-charge electric fields [9], and of non-linear terms, *e.g.* when the target populations in the collisional operator depend on the particle distribution function under evaluation. The most common strategy to overcome these difficulties assumes small departures from equilibrium caused by some agent χ_α, and involves the expansion of the particle distribution function in powers of χ_α around the equilibrium. The strategy is justified (i) in the case of the heavy ions, by highly-effective ion-neutral collisions that keep the system close to thermal equilibrium; (ii) in the case of the electrons, by assuming that the thermal (random) velocity is always larger than the drift velocity, due to the combined anisotropic effects of electromagnetic applied forces and pressure gradients.

When dealing with the electron Boltzmann equation (EBE), and in the absence of a magnetic field, it is usual to adopt one of the following expansions (the reader can refer to [29], for obtaining historical information on the subject, and to [30] for comprehensive information on the use of the EBE and the fluid equations to describe the transport of charged particles in nonequilibrium LTPs).

(a) A multi-term expansion in Legendre polynomials $P_l(\cos\theta)$ of the electron distribution function, considered either space-independent [25, 31–35] or steady-state, spatially 1-dimensional dependent [36–38]. Here, the angle θ defines the spatial orientation of the velocity vector $\vec{v}_e$ with respect to the polar direction of the total anisotropy (produced by electric fields and density gradients). Additionally, we can assume that the time-evolution or the space-evolution of the electron distribution function is due to the electron density growth, *e.g.* according to $n_e(t) \propto \exp(\langle\nu_{\rm ion}\rangle t)$ or $n_e(z) \propto \exp(\alpha z)$ (in the latter case, considering the sole action of an electric field along direction z). Under these conditions, the electron distribution function writes

$$F_e(z, \vec{v}_e, t) = \sum_{l=0}^{\infty} F_e^l(z, v_e, t) P_l(\cos\theta) \quad , \tag{18}$$

where the functions $F_e^l(z, v_e, t)$ depend only on the absolute value of the velocity.

(b) An expansion of the electron distribution function on the consecutive space gradients of the electron density [39,40]. In this case, F_e depends on $(\vec{r}, t)$ only through the density $n_e(\vec{r}, t)$, and the corresponding expansion is

$$F_e(\vec{r}, \vec{v}_e, t) = \sum_{l=0}^{\infty} F_e^{(l)}(\vec{v}_e) \overset{l}{\odot} \left(-\frac{\partial}{\partial \vec{r}}\right)^l n_e(\vec{r}, t) \quad . \tag{19}$$

Here, the expansion coefficients $F_e^{(l)}(\vec{v}_e)$ are tensors of order l depending only on $\vec{v}_e$, and $\overset{l}{\odot}$ indicates a l-fold scalar product [39].

The EBE that arises from using the previous expansions allows deducing the expressions of several important electron macroscopic properties, such as transport parameters and rate coefficients. For example, the electron reduced mobility $\mu_e n_0$, the electron reduced free-diffusion transverse coefficient $D_e n_0$ and the reduced Townsend ionisation coefficient α/n_0 can be obtained in the framework of a two-term expansion in Legendre polynomials, using the following equations

$$\mu_e n_0 = -\frac{1}{n_e}\frac{e}{3m_e}\int_0^\infty \frac{1}{\sigma_m}\frac{\partial F_e^0}{\partial v_e} 4\pi v_e^2 dv_e \tag{20a}$$

$$D_e n_0 = \frac{1}{n_e}\frac{1}{3}\int_0^\infty \frac{1}{\sigma_m} F_e^0 4\pi v_e^3 dv_e \tag{20b}$$

$$\frac{\alpha}{n_0} = \frac{\langle \nu_{\text{ion}} \rangle / n_0}{\mu_e E} = \frac{(1/n_e)\int_0^\infty \sigma_{\text{ion}} F_e^0 4\pi v_e^3 dv_e}{\mu_e E} \quad . \tag{20c}$$

Electron macroscopic quantities, such as the ones given by equations (20*a*)-(20*c*), are at the core of a popular strategy to determine complete cross section sets in gaseous electronics [41–43]. The strategy uses an iterative process to perform judicious adjustments to an initial compilation of data, as follows: (i) a set of cross sections is collected from the literature; (ii) the cross sections are used as input data to calculate electron distribution functions and to evaluate electron transport parameters and rate coefficients (from expressions such as (20*a*)-(20*c*)); (iii) the magnitudes of the cross sections are adjusted (within experimental error or theoretical uncertainty, if possible), to improve the agreement between calculated and measured swarm data. Note that although such an iterative procedure embeds a global consistency check, since it relies on reproducing measured electron macroscopic properties, it cannot be used to ensure either the uniqueness of the cross section set or the validation of the cross section for any individual process.

3.3. Stationary and homogeneous two-term electron Boltzmann equation

One of the most popular approaches for solving the EBE, under time-independent (stationary) and space-independent (homogeneous) conditions, assumes that the electron distribution function is adequately represented by the first two terms of expansion (18)

$$F_e(\vec{v}_e) \simeq F_e^0(v_e) + F_e^1(v_e)\cos\theta \quad , \tag{21}$$

where F_e^0 and F_e^1 are termed the electron distribution function isotropic and anisotropic components, respectively. Equation (21) corresponds to the well-known *two-term approximation* of the electron distribution function [25, 31, 33, 44], which allows for insightful interpretations of the physical phenomena in weakly ionized gases. The isotropic component monitors the deviations from thermal equilibrium, described by a Maxwellian distribution function, providing information about the particle and the energy balance. The anisotropic component describes the influence of the electric field and the density gradients in the development of preferential directions

of transport, and the consequent deviation from the isotropic equilibrium. The two-term approximation (21) is valid in a situation of small anisotropies, corresponding to (i) electron-neutral mean-free-paths λ_e much smaller than any characteristic dimension Λ of the plasma container, i.e. $\lambda_e \ll \Lambda$; and (ii) an energy gain from the electric field E, between collisions, much smaller than the electron kinetic energy $u = m_e v_e^2/2$, i.e. $eE\lambda_e \ll u$. The homogeneous two-term approximation neglects also the effects of transport by diffusion, in addition to assuming small energy gains due to drift under the action of the electric field, hence its validity is limited to high pressures, typically $\gtrsim 10^3$ Pa.

Introducing the two-term expansion (21) into the EBE (15), while assuming stationary and homogeneous conditions, using the orthogonality properties of the Legendre polynomials and changing variables from velocity space to energy space, it is possible to decompose (15) in the following set of coupled equations [25, 26, 33, 44]

$$-\frac{d}{du}\left[\frac{eE}{n_0}\frac{u}{3}f^1(u)\right] = \frac{1}{n_0}\sqrt{\frac{mu}{2}}\left(\frac{\partial f^0(u)}{\partial t}\right)_{\text{coll}} \equiv C_{\text{coll}} \tag{22a}$$

$$f^1(u) = \frac{eE}{n_0}\frac{1}{\sigma_m(u)}\frac{df^0(u)}{du} \quad . \tag{22b}$$

Here, the components of the electron distribution function have been renormalized as probability distribution functions satisfying $\int_0^\infty f^0(u)\sqrt{u}du = 1$, thus implying the following relationship $n_e\, f^0(u)\sqrt{u}du \equiv F_e^0(v_e)\, 4\pi v_e^2 dv_e$. Equation (22*a*)-(22*b*) is a continuity equation in energy space for the isotropic component $f^0(u)$, now termed the electron energy distribution function (EEDF), and it expresses the local balance between the electron energy gained from the applied electric field due to the microscopic drift-flux $f^1(u)$, and the electron energy lost in collisions.

The collisional term C_{coll} can be evaluated after a lengthy treatment of the different types of binary collisions considered: (i) electron-neutral elastic collisions, involving an exchange of kinetic energy only, which term is obtained from a correction to the Lorentz gas model [22, 25]; (ii) electron-neutral inelastic collisions, where the electrons give up part of their energy into the excitation of electronic, vibrational or rotational states; (iii) electron-neutral superelastic collisions, where the electrons receive energy in assisting an excited state to return to a lower energy state; (iv) electron-electron collisions, promoting a redistribution of the electron energy among the high- / low- energy populations, which term can be obtained from the Fokker-Planck equation (17) [45]. The expressions for the various collisional terms are as follows

$$C_{\text{e-o,el}} = \frac{d}{du}\left[\frac{2m_e}{M}u^2\sigma_{m,\text{el}}(u)\left(f^0(u) + k_B T_g \frac{df^0(u)}{du}\right)\right] \tag{23a}$$

$$C_{\text{e-o,inel}} = \sum_{i,j}\delta_i\left[(u+u_{ij})\sigma_{ij}(u+u_{ij})f^0(u+u_{ij}) - u\sigma_{ij}(u)f^0(u)\right] \tag{23b}$$

$$C_{\text{e-o,sup}} = \sum_{j,i}\delta_j\left[(u-u_{ij})\sigma_{ji}(u-u_{ij})f^0(u-u_{ij}) - u\sigma_{ji}(u)f^0(u)\right] \tag{23c}$$

$$C_{\text{e-e}} = \frac{d}{du}\left[2\nu_{ee}u^{3/2}\left(I(u)f^0(u) + J(u)\frac{df^0(u)}{du}\right)\right] \quad , \tag{23d}$$

where $I(u)$ and $J(u)$ are the relevant Spitzer integrals [25, 44], and $\nu_{ee} \equiv 4\pi \left[e^2/\left(4\pi\varepsilon_0 m_e\right)\right]^2 \ln\Lambda_c / v_e^3 n_e$, with $\ln\Lambda_c$ the Coulomb logarithm ($\Lambda_c \equiv 12\pi n_e \lambda_D^3$). Note that the elastic and e-e collisional terms ($23a$) and ($23d$) are written in a continuous form, similar to that of the electric-field heating term on the left-hand side of ($22a$), since these highly-frequent mechanisms are responsible for small variations in the electron energy. Note further that the effects of electron inelastic and superelastic collisions with rotational levels can also adopt a continuous approximation, due to the small energy separation between these levels. Again, the continuous expression for the rotational collisional term is similar to that of the elastic ($23a$), and details about its deduction can be found in [22, 41, 45, 46].

The homogeneous equation ($22a$)-($22b$) neglects any loss of electrons due to transport by diffusion. For consistency, one must also neglect the new electrons produced by ionisation, since the rate of appearance of these new electrons should be exactly compensated by the loss rate given by the missing diffusion term. In this case ionisation must be treated like an ordinary excitation process and, indeed, the inelastic and superelastic collision terms ($23b$) and ($23c$) are written for binary collisions that conserve the number of particles involved. The reader should refer to [32, 47–49] for information on expressions for electron ionisation collisions with production of secondary electrons.

The two-term EBE provides information also on the typical relaxation times of the electron distribution function components. By observing equation ($22a$)-($22b$), together with the usually dominant elastic collision term ($23a$), one concludes that the relaxation to equilibrium of the anisotropic component, due to transport effects, occurs much faster than the corresponding relaxation of the isotropic component, due to elastic collisions, noting the relationship between the corresponding electron-neutral collision frequencies $\nu_m \simeq \nu_{m,\mathrm{el}} \gg (2m_e/M)\nu_{m,\mathrm{el}}$ ($\nu_m \equiv n_0 \sigma_m (2u/m_e)^{1/2}$ and $\nu_{m,\mathrm{el}} \equiv n_0 \sigma_{m,\mathrm{el}} (2u/m_e)^{1/2}$).

For a given gas, in which the electron-neutral cross sections are known, equation ($22a$)-($22b$) is solved as a function of the reduced electric field E/n_0, the gas temperature T_g, the fractional population densities δ_i and δ_j of the pertinent excited states (in case stepwise inelastic and superelastic collisions are considered), and the electron density n_e (in case electron-electron collisions are considered). The numerical solution involves the discretisation of ($22a$)-($22b$) in the energy grid adopted, and the inversion of the corresponding matrix, which is diagonal-dominant (due to the continuous terms) and sparse (due to the collisional discrete terms).

As an illustration, figure 3 shows calculated EEDFs in argon at $T_g = 300$ K, for reduced electric fields $10^{-25} \leq E/n_0 \leq 10^{-19}$ V m^2. The results were obtained solving ($22a$)-($22b$) with the numerical tool LoKI-B [50], considering only elastic and inelastic electron collisions with ground-state atoms, taking the Ar complete cross section set of the IST-Lisbon database with the LXCat open-access website [51, 52]. The figure shows that for $E/n_0 < 10^{-20}$ V m^2 the electric power is insufficient to produce plasma, since the EEDF does not reach the first excitation threshold of argon at ~ 10 eV, thus indicating that elastic collisions are the main electron-neutral scattering mechanism in this case. In fact, for extremely low values of E/n_0 the neutral gas acts

as a heat source for the electrons, in which case the EEDF is a Maxwellian distribution function at $T_g = 300$ K. Above 10^{-20} V m^2, the EEDFs exhibit a low-energy (*body*) region and a high-energy (*tail*) region, separated by the ~ 10 eV threshold regardless of the E/n_0 value, which variations cause changes only in the shape of the EEDF in these regions.

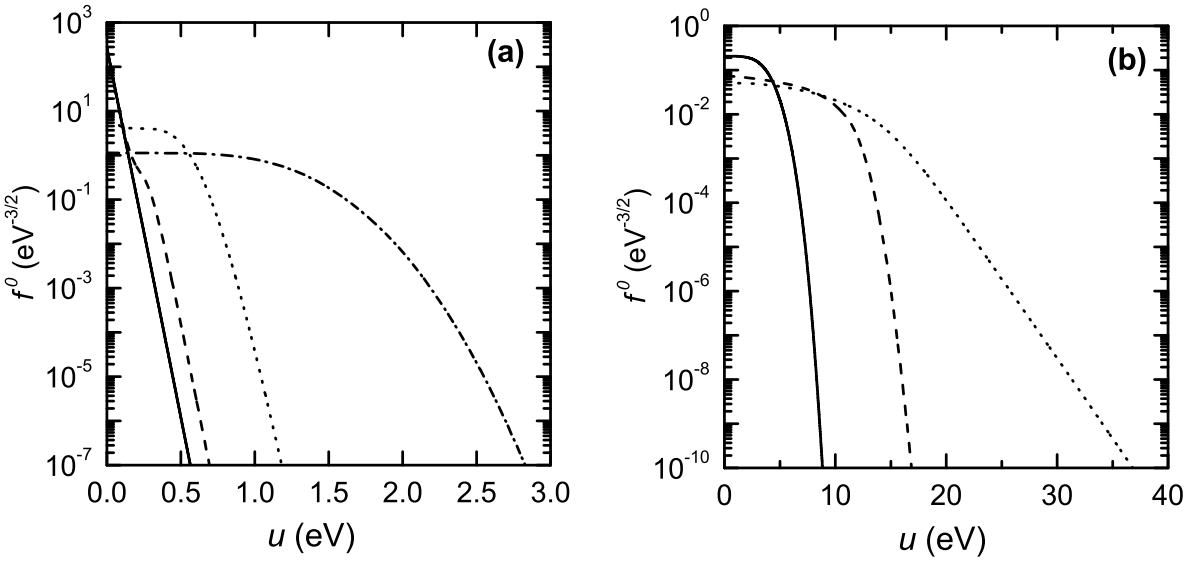

Figure 3. Electron energy distribution functions in Ar for $T_g = 300$ K and the following values of E/n_0 (V m^2): (a) 10^{-25} (solid line), 10^{-24} (dashed), 10^{-23} (dotted), 10^{-22} (dashed-dotted); (b) 10^{-21} (solid), 10^{-20} (dashed), 10^{-19} (dotted).

Figure 4 shows calculated EEDFs and vibrational distribution functions (VDFs) δ_v in molecular nitrogen, for $E/n_0 = 10^{-19}$ V m^2, $T_g = 300$ K, and various values of the so-called characteristic vibrational temperature T_v in the range $2000 - 4000$ K. The vibrational temperature is defined from a Boltzmann fit to the lowest four vibrational levels, and in practice it is associated with the ionisation degree n_e/n_0 that changes the intensity of the vibrational pumping. As before, the results were obtained solving (22*a*)-(22*b*) with the numerical tool LoKI-B [50], this time considering elastic and electronic inelastic electron collisions with ground-state molecules (adopting the IST-Lisbon complete cross section set for N_2 [51, 52]), as well as inelastic/superelastic collisions with the vibrational levels of ground-state N_2(X,v). For consistency, the EBE is solved together with the system of rate balance equations determining the populations δ_v, using the kinetic scheme and data presented in [53,54]. It is seen that the EEDF steeply drops at around 2.5 eV, due to the sharp peak of the total vibrational excitation cross section at about this energy, which acts as a vibrational barrier that prevents electrons from attaining higher energies. As T_v increases, the signature of the potential barrier is mitigated (with a decrease in the body of the EEDF and a simultaneous increase in its tail), due to electron heating by superelastic electron-vibration collisions, promoted by the enhanced VDF. These results show the need for a coupled solution between the

electron and the vibrational kinetics, in gases where vibrational levels play a key role in defining energy exchanges.

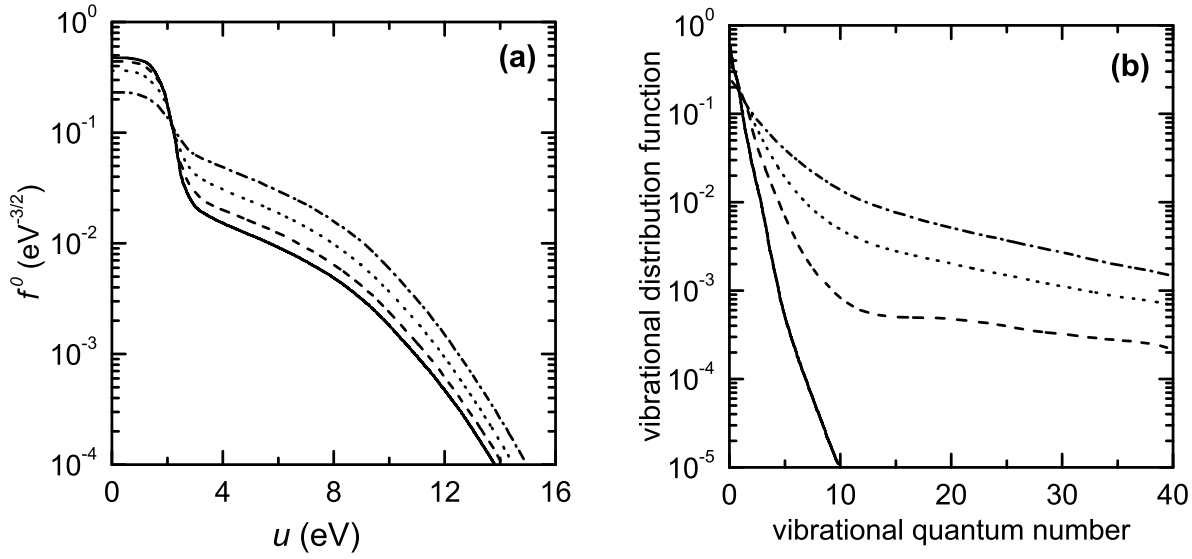

Figure 4. Electron energy distribution functions (a) and vibrational distribution functions (b) in N_2 for $E/n_0 = 10^{-19}$ V m^2, $T_g = 300$ K and the following values of T_v (K): 2000 (solid lines), 3000 (dashed), 4000 (dotted) and 6000 (dashed-dotted).

3.4. Complements

The study of the EBE presented in the previous sections was limited to situations where the force acting on the electrons was due to a time-independent direct-current (DC) electric field. This treatment can be generalized (i) to situations where the applied electric field has also a high-frequency (hf) component at frequency $\omega \gg \nu_m$ [26, 32, 44, 55], in which case the electron distribution function (18) is expanded also in Fourier series in time, and (ii) to magnetized plasmas [25, 26], in which case the total force acting on the electrons has also a magnetic component that breaks the azimuthal symmetry around the total anisotropy direction. In this situation, the electron distribution function must be expanded using the associated Legendre polynomials $P_l^m(\cos\theta)$, where the m-index relates to the dependence on the azimuthal coordinate.

The previous study was limited also to high pressure situations, when the input power from the electric field compensates the power lost in elastic and inelastic electron collisions. This condition corresponds to the *local field approximation* (LFA), based on the assumption $f^0(\vec{r}, u) \simeq n_e(\vec{r}) f^0(u)_{|E/n_0(\vec{r})}$, valid in a homogeneous plasma or when the spatial evolution of the electron kinetic quantities proceed through a sequence of nearly homogeneous states. The LFA requires a very short relaxation length of the electrons in comparison with the spatial change of the electric field, a situation favoured by relatively high pressures (or large plasma dimensions).

In non-homogeneous plasmas at sufficiently low pressure, so that the energy relaxation length of the electrons exceeds the plasma dimensions, the total energy $\epsilon = u - eV(r)$ (where $V(r)$ is the radial space-charge electric potential [9]) remains nearly constant during the electron displacement, and the distribution function $f^0(r, u)$ becomes totally non-local. These are the basis of the *non-local approach* [56, 57], valid when spatial diffusion and space-charge terms are dominant, in which case the EBE can be expressed in the total energy (becoming a constant of motion) rather than in the kinetic energy.

In the case of intermediate pressures (typically ~ 100 Pa [58]), where neither the LFA nor the non-local approach are valid, one should attempt the resolution of the spatially-dependent EBE [59, 60]. However, this cumbersome task can be avoided if the goal is limited to the description of the spatial-dependence of the electron macroscopic parameters, for use in hybrid models. In this case it is possible to adopt the *local mean energy approximation* (LEA) [58, 61, 62] which assumes that the spatial dependence of the EEDF is introduced via the electron mean energy $\varepsilon(\vec{r})$, $f^0(\vec{r}, u) \simeq n_e(\vec{r}) f^0(u)_{|\varepsilon(\vec{r})}$. In practice, for a 1-dimensional case, the LEA can be employed within the fluid module (see section 4) of an hybrid model as follows: (i) the homogeneous two-term EBE is solved at different electric fields; (ii) the results so obtained are used to construct a table of electron parameters as a function of the electron mean energy $\varepsilon_{\text{Boltz}}$, and (iii) the radial distribution of the electron mean energy $\varepsilon(r)$, obtained from the solution to the fluid model, is used to deduce the spatial profiles of the electron parameters by resorting to the table constructed in (ii) (at each r, looking for the match $\varepsilon(r) = \varepsilon_{\text{Boltz}}$).

4. Plasma fluid models

Section 3 showed that large amount of information can be obtained by solving the kinetic equations for the charged particles in a plasma. This approach is particularly interesting in the case of the electrons, since it provides a detailed description of the energy exchanges with the excitation source and with the heavy-species of the gas/plasma medium, which can be extremely relevant for the correct modelling of the system. However, section 3 showed also that the solution to the Boltzmann equation involves several approximations, introduced to ensure the feasibility of the problem within acceptable calculation times. In particular, because the focus of the particle kinetic studies is usually on the energy description, the space-time dependence of the particle distribution function is often neglected or at least simplified. As mentioned, a possible outcome for these limitations leverages on an hybrid approach, by using flexible and mixed calculation modules adapted to the specific features of the different problem components.

In this context, fluid models provide an adequate compromise solution between the inclusion of fundamental phenomena accounting for the dynamics of species and a space-time description of the plasma excitation setup, keeping the calculation burden within acceptable limits. In a fluid model, the plasma is treated from a macroscopic

point of view as a multi-fluid system of electrons, ions (both positive and negative), and neutrals (molecules, atoms, radicals), which are transported within a gaseous background. The model formulation to describe a nonequilibrium LTP, created and maintained by an electrical discharge, involves writing the hydrodynamic-like equations for the plasma species, noting the following two main differences with respect to an ordinary thermodynamic fluid. The first difference is that the transport of electrons and ions in the quasi-neutral plasma is affected not only by the externally applied field, but also by the electrostatic space-charge field that develops to control the charge separation within the discharge [9]. The self-consistent calculation of the space-charge field, as a function of the corresponding charge separation, requires the solution to Poisson's equation coupled to the hydrodynamic equations. The second difference is that a plasma is a reactive medium, within which species are generated and destroyed both in the volume and in interaction with the walls, in such a way that the ionisation rate must compensate for the particle loss-rate to the wall. The relationship between these rates defines a univocal discharge working-point, for a given set of discharge input parameters (pressure, power and geometrical dimensions), which must be self-consistently determined as an eigenvalue solution to the problem [61].

Next section will briefly deduce the hydrodynamic equations for the various plasma species k (where $k = \alpha$ refers to the charged particles e, i and $k = o$ refers to the neutral particles), by calculating the moments of the Boltzmann kinetic equation (15) [23,26,61], which involves a hierarchical integration of this equation in velocity space. Our attention will be devoted to gas/plasma systems created and maintained by electrical discharges at with negligible flow, where electrons and positive ions are transported in a quasi-immobile neutral gaseous background, under the action of drift (due to the electrostatic space-charge field) and diffusion (due to the natural density gradients that develop towards the discharge walls).

4.1. Fluid equations as moments of the Boltzmann equation

The moments of the Boltzmann equation are conservation laws for any quantity $\chi(\vec{r}, \vec{v}_k, t)$ associated with a plasma species k located at position $\vec{r}$ and velocity $\vec{v}_k$, at time t. In order to derive a macroscopic conservation law for this general quantity, equation (15) is multiplied by χ and integrated in velocity space, yielding (assuming velocity-independent external forces)

$$\frac{\partial}{\partial t}\left(n_k\langle\chi\rangle\right) - n_k\langle\frac{\partial\chi}{\partial t}\rangle + \sum_l \frac{\partial}{\partial x_l}\left(n_k\langle\chi v_{k_l}\rangle\right) - \sum_l n_k\langle\frac{\partial\chi}{\partial x_l}v_{k_l}\rangle - \sum_l n_k\langle\frac{\partial\chi}{\partial v_{k_l}}\rangle\frac{X_{k_l}}{m_k}$$
$$= \int_{\vec{v}_k}\chi\left(\frac{\partial F_k}{\partial t}\right)_{\text{coll}} d\vec{v}_k \quad , \tag{24}$$

where we have introduced the velocity-averaged value of χ

$$\langle\chi\rangle(\vec{r}, t) \equiv \frac{1}{n_k}\int_{\vec{v}_k}\chi(\vec{r}, \vec{v}_k, t)F_k(\vec{r}, \vec{v}_k, t)\, d\vec{v}_k \quad . \tag{25}$$

The equation for the conservation of the number-density, i.e. the continuity equation, is obtained by making $\chi = 1$ to give

$$\frac{\partial n_k}{\partial t} + \vec{\nabla} \cdot \vec{\Gamma}_k = S_k \quad , \tag{26}$$

where $\vec{\Gamma}_k \equiv n_k \vec{v}_{d_k}$ is the k-species flux, and the $\vec{\nabla}$ operator represents the gradient in configuration space.

By making $\chi = m_k \vec{v}_k$ and by using (26), one obtains the equation for the momentum conservation

$$\frac{n_k}{\nu_k} \frac{\partial \vec{v}_{d_k}}{\partial t} + \frac{n_k}{\nu_k} \left(\vec{v}_{d_k} \cdot \vec{\nabla} \right) \vec{v}_{d_k} \mp n_k \mu_k \vec{E} + D_k \vec{\nabla} n_k = - \left(n_k + \frac{S_k}{\nu_k} \right) \vec{v}_{d_k} \ , \tag{27}$$

with $\vec{E}$ accounting for the total (external $\vec{E}_{\text{ext}}$ and space-charge $\vec{E}_s$) electric field acting on the particles (the $\mp$ signs apply to positive ions and electrons, respectively), and where the momentum-transfer average frequency, for the collision between a k-species and a neutral species, is represented by $\nu_k \equiv \langle \nu_{m_k} \rangle$ for simplicity of the notation. Equation (27) was obtained for an inviscid plasma, by separating $\vec{v}_k$ into its drift and thermal components, i.e. $\vec{v}_k \equiv \vec{v}_{d_k} + \vec{v}_{\text{th}_k}$, the latter assumed quasi-isotropic.

It is possible to introduce specific simplifications to (27), according to the working conditions and the particular type of particles considered ($k = e, i, o$), namely: (i) under stationary conditions, by setting to zero the first term on the left-hand side; (ii) for moderate / high pressures, by taking $S_k \ll n_k \nu_k$, disregarding the corresponding term on the right-hand side; (iii) for the electrons and the neutrals, by neglecting the non-linear inertia term $\left(\vec{v}_{d_k} \cdot \vec{\nabla} \right) \vec{v}_{d_k}$, considering situations of negligible flow and recalling that the space-charge electric field mitigates the wall-oriented electron flux. Note that the opposite action of the space-charge field upon the positive ions, responsible for their acceleration nearby and towards the walls, requires retaining the non-linear term in (27); (iv) for the neutrals, by setting to zero the drift due to the electric field. The corresponding expressions are

$$\vec{\Gamma}_e = -n_e \mu_e \vec{E} - D_e \vec{\nabla} n_e \tag{28a}$$

$$\vec{\Gamma}_i = -\frac{n_i}{\nu_i} \left(\vec{v}_{d_i} \cdot \vec{\nabla} \right) \vec{v}_{d_i} + n_i \mu_i \vec{E} - D_i \vec{\nabla} n_i \tag{28b}$$

$$\vec{\Gamma}_o = -D_o \vec{\nabla} n_o \quad , \tag{28c}$$

with (28a), for the electrons, corresponding to the so-called *drift-diffusion approximation*; (28b), for the ions, further including the inertia term accounting for the spatial-transport of momentum; and (28c), for the neutrals, corresponding to the well-known Fick's law. In (28a), the electron transport parameters μ_e and D_e can be calculated by integrating the corresponding non-equilibrium EEDF, using (20a) and (20b), with a space-time variation as given by the LEA [58, 61, 62] (see section 3). For the ions and the neutrals one can usually assume equilibrium conditions, in which case $\mu_k = e/(m_k \nu_k)$ and $D_k = k_B T_k/(m_k \nu_k)$, with $m_k \langle v_{\text{th}_k} \rangle^2/2 \simeq \varepsilon_k = (3/2) k_B T_k$.

Finally, by making $\chi = m_k v_k^2/2$ and by adopting a set of approximations similar to that used in (27), one obtains the equation for the energy conservation

$$\frac{\partial}{\partial t}\left(n_k \varepsilon_k\right) + \vec{\nabla}\cdot\vec{\Gamma}_{\varepsilon_k} \mp e\vec{E}\cdot\vec{\Gamma}_k + \Theta_k = 0 \tag{29}$$

where the k-species energy flux is given by

$$\vec{\Gamma}_{\varepsilon_k} = \pm n_k \varepsilon_k \mu_{\varepsilon_k}\vec{E} - D_{\varepsilon_k}\vec{\nabla}\left(n_k\varepsilon_k\right) \quad . \tag{30}$$

Again, the $\mp$ / $\pm$ signs in (29) / (30) apply to positive ions and electrons, respectively. The different terms in equation (29) represent, in order, the time-variation of the power density; the power density gained / lost in convection (due to drift and diffusion phenomena); the power density transferred by the electric field; and the power lost in collisions $\Theta \equiv -\int_{\vec{v}_k} m_k v_k^2/2\left(\partial F_k/\partial t\right)_{\text{coll}}\, d\vec{v}_k$. As for the electron-particle transport parameters, μ_{ε_e} and D_{ε_e} can be obtained by adequate integration of the EEDF, with a space-time variation given by the LEA [61]; for a Maxwellian distribution function and an energy-independent collision frequency ν_k, the electron-energy transport parameters satisfy the simple relationships $\mu_{\varepsilon_k} = (5/3)\mu_k$ and $D_{\varepsilon_k} = (5/3)D_k$. Often, in plasma fluid models, equations (29) and (30) are solved for the electrons and the heavy-species (ions and neutrals) to deduce the space-time variation of the electron mean energy and the gas temperature, respectively, assuming thermalisation between the ions and the neutrals at T_g.

In the case of a stationary homogeneous plasma, the first two terms of (29) can be neglected, yielding (for electrons and ions, and after substitution of the corresponding particle drift-flux)

$$\sigma_\alpha E^2 = \Theta_\alpha \quad , \tag{31}$$

which expresses the LFA (see section 3), when the power gained from the electric field balances the power lost in collisions.

4.2. Transport in a plasma column controlled by diffusion

In principle, the validity domain of plasma fluid models is limited to (i) a Debye length smaller than the discharge dimension, $\Lambda/\lambda_D \gg 1$, to ensure the typical conditions of uncorrelated LTPs (see section 3). In this case, the charged-particle density is sufficiently high to shield the effects of space-charge separation, hence providing the conditions for an ambipolar motion, i.e. a coupled transport of electrons and ions by diffusion, controlled by a common ambipolar diffusion coefficient; (ii) mean-free-paths smaller than the characteristic discharge dimension, $\Lambda/\lambda_k > 1$, to ensure a proper definition of macroscopic parameters within the volume elements along the motion-path of the particles. This condition is satisfied at moderate / high pressures (and large discharge dimensions), for which charge separation is mitigated due to the enhanced collisionality of the plasma. This section briefly reviews the description of the transport of charged particles in a plasma column controlled by diffusion, i.e. under ambipolar situations satisfying $\Lambda/\lambda_D \gg 1$.

The *classical ambipolar diffusion regime*, a high-pressure limit for the transport of charged particles ($\Lambda/\lambda_k \gg 1$), was treated first by Schottky [63] who deduced the classical ambipolar diffusion coefficient D_a, by considering electrons in Boltzmann equilibrium with the electrostatic potential and positive ions with non-inertial behaviour. These conditions can be obtained from (28*a*)-(28*b*), by neglecting the ionic non-linear term and by further assuming quasi-neutrality ($n_e = n_i \equiv n$), proportionality ($\vec{\nabla} n_e/n_e = \vec{\nabla} n_i/n_i$) and congruence ($\vec{\Gamma}_e = \vec{\Gamma}_i \equiv \vec{\Gamma}$), to obtain [9]

$$\vec{\Gamma} = -D_a \vec{\nabla} n \tag{32a}$$

$$\vec{E}_s \simeq -\frac{D_e}{\mu_e}\frac{\vec{\nabla} n}{n} \tag{32b}$$

$$D_a \simeq D_i \frac{D_e/\mu_e}{k_B T_i/e} \quad . \tag{32c}$$

As the gas pressure decreases, and the level of collisionality with neutrals reduces, diffusion becomes less important in the ambipolar transport of charged particles. At very low pressures, one can assume that the electrons are in Boltzmann equilibrium with the space-charge potential, and that the positive ions are freely accelerated by the space-charge field, from the positions where they are produced to the discharge wall, with a velocity distribution defined by energy conservation. These are the main hypotheses of the so-called *free-fall regime*, a low-pressure limit for the ambipolar transport of charged particles ($\Lambda/\lambda_k \ll 1$), which was firstly explored by Tonks and Langmuir [64] for the quasi-neutral plasma region.

Strictly, the description of the low-pressure free-fall regime is out of the scope of a plasma fluid model. However, because both models (classical-ambipolar and free-fall) focus on the neutral plasma, not attempting to describe the charge-separation region, one might consider using a fluid-type formulation to capture the evolution with pressure of the charged-particle ambipolar transport. Indeed, Self and Ewald [65] proposed a unified transport theory for a plasma column controlled by ambipolar motion at intermediate pressures, using the fluid equations (26) and (28*a*)-(28*b*) for electrons and ions written in planar and cylindrical geometries, which gives results in agreement with the classical-ambipolar and the free-fall limits, thus bridging the gap between these two regimes in a continuous way. The results of Self and Ewald were later expressed by Ferreira and Ricard [66] in the convenient form of an effective diffusion coefficient for the electrons D_{se} dependent on Λ/λ_i (see figure 5), which can be used to generalize (32*a*) for different pressures as $\vec{\Gamma}_e = -D_{se}\vec{\nabla} n_e$.

4.3. Structure and examples

The typical plasma fluid model solves the hydrodynamic equations (26), (28*a*)-(28*c*), and (29)-(30), coupled to Poisson's equation for the space-charge field [58, 61, 65, 67–69]

$$\vec{\nabla} \cdot \vec{E}_s = \frac{e\,(n_i - n_e)}{\varepsilon_0} \quad , \tag{33}$$

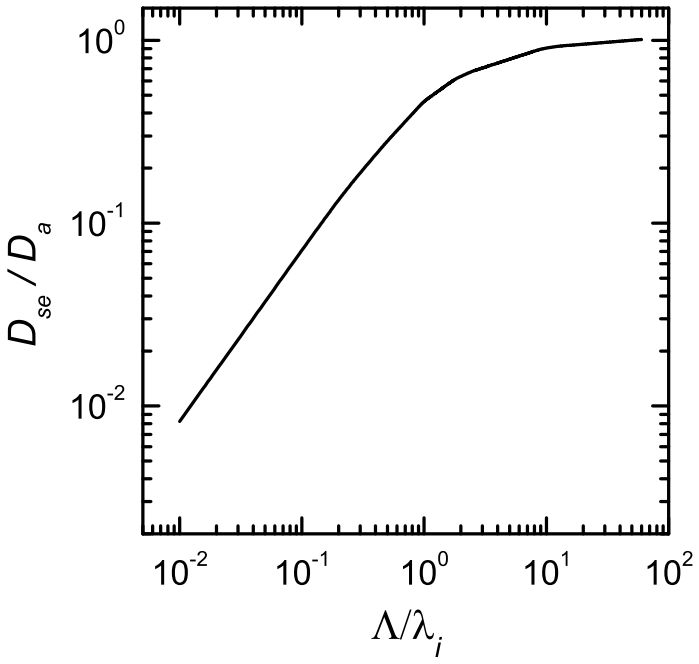

Figure 5. Ratio of the electron effective diffusion coefficient to the ambipolar diffusion coefficient, as a function of the ratio of the characteristic diffusion length to the ion mean-free-path, according to [65, 66].

yielding the space-time distribution of the densities and the fluxes of the different plasma species, the electron mean energy and the energy flux, and the space-charge electrostatic field.

The numerical solution of the plasma fluid model involves (i) the discretisation of its equations in a multidimensional $\vec{r}$-grid, preserving the particle and energy conservation described by the corresponding balance equations, taking into account adequate flux boundary-conditions [70, 71]; (ii) the imposing of boundary conditions for the particle and energy fluxes, eventually accounting also for the presence of surface charges (together with symmetry conditions for the derivatives of scalar quantities, if applicable) [61]; (iii) the solution of the discretized set of equations for given discharge input parameters (gas pressure and temperature, geometrical dimensions), using iterative algorithms due to the intrinsic time-dependence of the physical problem (*e.g.* when describing capacitively coupled radio-frequency (CCRF) discharges [70, 72]), or simply because of its non-linearity [61]; (iv) the eigenvalue calculation of the discharge working-point, corresponding to the value of the reduced electric field E/n_0 (or power) consistent with the product of the gas density by the discharge dimension $n_0\Lambda$, considering the closure / boundary condition for some quantity that defines the plasma excitation (*e.g.* discharge current, electric potential, electron density). For example, in DC discharges this last step corresponds to obtaining the reduced field that yields an electron-density distribution compatible with the value imposed for the discharge current $I_{\rm DC} = f(E_{\rm ext}/n_0, n_e)$ at given working conditions (see figure 6 adapted from [61]);

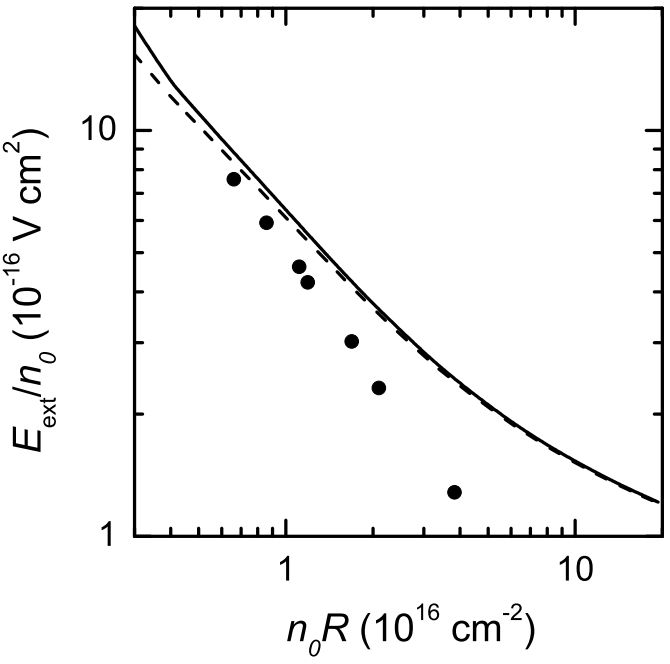

Figure 6. Reduced electric field $E_{\rm ext}/n_0$, axially applied to a DC helium discharge at $T_g = 300$ K, as a function of the product n_0R (with $R = 2.405\Lambda$ the discharge radius in cylindrical geometry). The curves are calculations for $I_{\rm DC} = 50$ mA (solid line) and 200 mA (dashed). The points are measurements of Kaneda [73] for $I_{\rm DC} = 30$ mA.

whereas in CCRF discharges it defines the effective electric power $W_{\rm eff}$ compatible with the electron density and the boundary condition for the rf-potential $V_{\rm rf_{|bound}}$, such that $W_{\rm eff} = f[n_e(V_{\rm rf_{|bound}}), V_{\rm rf_{|bound}}]$ at given working conditions (see figure 7 from [74]).

The situation is easier to understand in DC discharges, where the electron-particle production can be described by an expression combining the continuity equation (26) and the ambipolar flux $\vec{\Gamma}_e = -D_{se}\vec{\nabla}n_e$,

$$\frac{\langle\nu_{\rm ion}^{\rm eff}\rangle}{n_0} = \frac{D_{se}n_0}{(n_0\Lambda)^2} \qquad (34a)$$

$$-\frac{\nabla^2 n_e}{n_e} \equiv \frac{1}{\Lambda^2} \quad , \qquad (34b)$$

where $(34a)$ is written as function of the typical reduced parameters $\langle\nu_{\rm ion}^{\rm eff}\rangle/n_0$, $D_{se}n_0$ and $n_0\Lambda$. Here, $\langle\nu_{\rm ion}^{\rm eff}\rangle$ is defined as an effective ionisation frequency that gives the net production rate of electrons $S_e \equiv n_e\langle\nu_{\rm ion}^{\rm eff}\rangle$, and Λ is the characteristic diffusion length defined as the solution to the differential equation $(34b)$. Equation $(34a)$ is the well-known Schottky condition [63], expressing that the ionisation rate must compensate for the particle loss-rate to the wall. For given discharge input parameters (n_0 and Λ) and for a calculated distribution of the electron density, this equation determines the eigenvalue E/n_0 consistent with the required net production rate of electrons.

The solution of the plasma fluid model gives also the neutral densities n_o. These densities are needed to calculate the different source terms S_k, defined according to

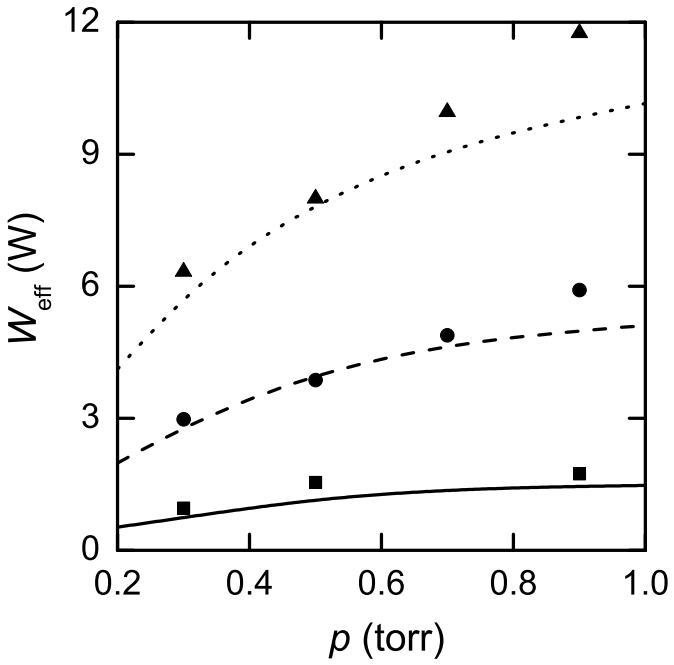

Figure 7. Effective electrical power coupled to the plasma, as a function of pressure, for a CCRF discharge with 124 mm diameter and 30 mm interelectrode distance, at $V_{\mathrm{rf}_{|\mathrm{bound}}} = 100$ V and $T_g = 323$ K. The curves (simulations) and the points (measurements) were obtained at frequencies of 13.56 MHz (solid curves and squares), 27.12 MHz (dashed and circles), and 40.68 MHz (dotted and triangles). Reprinted from [74], with the permission of AIP Publishing.

the reaction mechanism adopted for the collisional-radiative creation / destruction of species k (see section 5). If the reaction mechanism involves a complex chemistry, the dynamics of neutral species is often described using the algebraic form of the rate-balance equations resulting from (26) and (28c), i.e.

$$\frac{\partial n_o}{\partial t} \simeq S_o - \frac{D_o}{\Lambda^2} n_o \quad , \tag{35}$$

which correspond to the basic equations of many collisional-radiative models.

5. Plasma global models

5.1. Set of equations

In global models, also called 0D chemical kinetics models, the conservation equations for the number density of the various plasma species, as used in the plasma fluid model (see (26)) are reduced to simple balance equations, based on production and loss terms as defined by the chemical reactions, hence typically neglecting the transport term of (35), although methods have been developed to include the effect of transport losses (as discussed in more detail in section 5.3.3 below). The simplest form of these equations

can be written as

$$\frac{dn_k}{dt} = \sum_j \{(a_{kj}^{(2)} - a_{kj}^{(1)}) k_j \prod_l n_l^{a_{lj}^{(1)}}\} \quad , \tag{36}$$

where $a_{kj}^{(1)}$ and $a_{kj}^{(2)}$ are the stoichiometric coefficients of species i, as they appear on the left- and right-hand sides of a reaction j, respectively.

Besides, an electron energy conservation equation can be solved to calculate the average electron energy, again based on production and loss terms, as defined by the power deposition or by the electric field, and the chemical reactions, respectively

$$\frac{d(n_e \varepsilon_e)}{dt} = Q_{\text{ext}} - \sum_s \frac{3}{2} n_e \nu_s k_B \frac{2m_e}{M_s}(T_e - T_g) + \sum_j n_e k_j n_j \Delta\varepsilon_j \quad , \tag{37}$$

where Q_{ext} is a source term corresponding to the external power input and $\Delta\varepsilon_j$ is the change in electron energy caused by electron-impact reaction with species j. The electron temperature is then typically obtained from $k_B T_e = (2/3)\varepsilon_e$.

To solve (36) one needs to calculate the rate coefficients k_j. The rate coefficients for electron-induced processes, such as ionisation, excitation and dissociation, are typically obtained from the corresponding energy-dependent cross sections, multiplied by the EEDF, i.e.

$$k_j = \left(\frac{2}{m_e}\right)^{1/2} \int_0^\infty u \sigma_j(u) f^0(u) du \quad . \tag{38}$$

The EEDF is calculated with a Boltzmann solver, usually integrated in such global models, in which case there is no strict need to solve the electron-energy conservation equation (37). The rate coefficients of the other chemical reactions, i.e., between the neutral species or ions, depend on the gas temperature and are typically calculated from Arrhenius equations, using data adopted from literature.

Usually, no energy balance equation is solved for the heavy particles, as they are assumed to have the same temperature as the gas. Thus, the gas temperature can be calculated from a general energy conservation equation for the heavy particles. Assuming isobaric conditions and neglecting the spatially dependent terms, this gives

$$N \frac{\gamma k_B}{\gamma - 1} \frac{dT_g}{dt} = P_{e,el} - \sum_j R_j \Delta H_j + P_{ext} \quad , \tag{39}$$

where $N = p/(k_B T_g) = \sum_k n_k$ is the total gas density (i.e. the sum of the number densities of all heavy species), $P_{e,el}$ is the power transferred from the electrons to the heavy particles by elastic collisions, corresponding to the second term on the right-hand side of (37), R_j is the rate of reaction j, ΔH_j is the heat released or consumed in the reaction j, $\gamma = C_p/C_v$ is the ratio of the specific heat at constant pressure C_p to the specific heat at constant volume C_v, and P_{ext} is the heat gained or lost due to the energy exchanges with the surroundings. Often, the gas temperature is simply defined as input parameter of the global model (see below).

Global models are quite easy to program. Besides, there are some codes available within the plasma community for global model calculations. The most commonly

used are ZDPlaskin, developed by Pancheshnyi *et al* [75], GlobalKin, developed by Kushner and coworkers [76, 77], for which a commercial application, Quantemol-P, is also developed with a graphical user interface [78], as well as a global model within the PLASIMO software, developed by van Dijk and coworkers [79]. Recently, a very interesting tutorial review paper on global models was published by Hurlbatt *et al* [80].

5.2. Some examples of typical application fields

Global models are the most logical method of choice for describing the detailed plasma chemistry in complex gas mixtures, without too much computational effort. They are often used to describe the chemistry of different gas/plasma systems with potential interest for different applications (*e.g.* plasma medicine, environmental control, ...). Eliasson and Kogelschatz applied a global model to describe the chemistry of ozone formation in dry air, considering 30 species and 143 reactions [81]. Kossyi *et al* further expanded that chemistry to 450 reactions [82]. Gentile and Kushner developed a plasma chemistry set for humid air, using 56 species and 400 reactions [83]. Sakiyama *et al* applied two coupled global models for plasma medicine applications, to describe a surface microdischarge with 50 species and 600 reactions [84]. Liu *et al* reported a global model for He/H_2O, containing 46 species and 577 reactions, and also suggested several reduced chemistries [85]. Waskoenig *et al* proposed such a reduced set with 16 species and 116 reactions for a He/O_2 mixture [86]. The chemistry of atmospheric-pressure plasma jets was further studied with a global model by Murakami *et al* for a $He/O_2/N_2/H_2O/CO_2$ mixture with 59 species and 1048 reactions [87, 88]. Van Gaens and Bogaerts applied a global model for several types of argon plasma jets flowing into humid air, considering 84 species and 1880 reactions, and also proposed several reduced sets [89–92]. Finally, Schmidt-Bleker *et al* applied a global model with a reduced reaction scheme, to model the chemistry of the effluent of the kINPen plasma jet, without including the electron dynamics [93].

Furthermore, global models have also been used for modelling plasma-liquid interactions, where the approach can be extended to the liquid phase. For instance, van Gils *et al* presented a global model for the liquid-phase chemistry upon plasma treatment, assuming certain values for the fluxes of O_3, NO, OH originating from the plasma, in order to elucidate the bacterial inactivation mechanisms in the liquid phase [94]. Hamaguchi and coworkers developed a global model to describe the behaviour of reactive species in pure water (with dissolved O_2 and N_2 in equilibrium with air) exposed to an atmospheric-pressure plasma [95]. Lietz and Kushner applied a global model for plasma-liquid interaction and liquid-phase chemistry, and showed that this approach is very useful when multiple timescales (from a few ns during the discharge pulses to many minutes for reactions in the liquid) have to be addressed [96]. Finally, Kong and coworkers recently developed a combined global model for the plasma phase and 1D fluid model for the liquid phase, to understand the chemistry in plasma-activated solutions [97].

Also for gas conversion applications, global models are often the most suitable approach, because of the many different plasma species and chemical reactions that need to be described, and they have been used among others for describing CO_2 splitting in dielectric barrier discharges, microwave and gliding arc plasmas, including the role of the CO_2 vibrational levels, as well as for CO_2/CH_4, CO_2/N_2 and CO_2/H_2O mixtures (*e.g.*, [98–112]).

Other application fields where global models have shown to be very useful include thruster design [113, 114], high-power impulse magnetron sputtering [115, 116], and plasma processing [117–120].

5.3. Advantages and limitations

5.3.1. Detailed plasma chemistry and associated uncertainties

It is clear that global models are very suitable for describing a detailed plasma chemistry, as mentioned above. Hurlbatt *et al* [80] showed that the number of chemical reactions to be accounted for rises more or less linearly with the number of species included in the model. For mixtures of He with O_2, or (humid) air, approximately 1000 reactions are typically included for about 50 species, but this number can even reach up to nearly 2000 reactions for about 100 species, as also outlined above. These species include various types of molecules, radicals, ions and (electronically and vibrationally) excited species, besides the electrons.

As a consequence, global models are very useful for chemical reaction pathway analysis, to study the most important production and loss processes for various species, as illustrated *e.g.* for plasma medicine applications [92], as well as for gas conversion applications [109, 110]. They allow to obtain more insight in the limitations for the production of some species, and consequently, they also provide solutions on how to overcome these limitations.

The fact that global models typically describe a detailed plasma chemistry also points towards their main weakness, i.e., the need for accurate rate coefficients or cross sections for all these reactions. The latter are often subject to uncertainties, and this limits the accuracy and the predictive character of the global modelling results. Quite often multiple sources for the same reaction rate coefficients or cross sections can be found, which can differ significantly, and researchers not always refer to (or check) the original references, where the expressions of these rate coefficients were determined. Furthermore, the rate coefficients are often valid only for a certain range of the gas temperature or pressure, so one has to take care that they are used within this parameter range in the model. Ideally, the rate coefficients should include dependencies on the gas temperature and pressure. Furthermore, it should be realized that global models are mainly suitable at sufficiently high gas pressures, where collisions and chemical reactions are dominant.

The critical effect of the uncertainties in the rate coefficients and cross sections must therefore be taken into account when interpreting the results of global models,

and there is strong need for reliable data and for the adoption of verification and validation procedures when developing such models. This problem is common to all plasma models, but it is particularly critical in global models, where the aim is usually to study a complex chemistry. Turner was the first one to bring this issue to the attention of the low-temperature plasma community, for a helium-oxygen mixture [121–123]. He presented a MC model that uses a large number of different combinations of rate coefficients, generated randomly within the uncertainties associated with each of these rate coefficients. This provides a good estimation of the uncertainty on the model results, attributed to the rate coefficients. Recently, Berthelot and Bogaerts applied a similar methodology to a CO_2 plasma [124]. Figure 8 illustrates the electron temperature and the electron density as a function of time, for a CO_2 plasma at 300 K gas temperature, 2×10^4 Pa gas pressure and 200 W cm^{-3} power density, showing the uncertainty in the calculation results, based on the uncertainties in the rate coefficients used in the model. For a more detailed explanation, the reader should refer to [124].

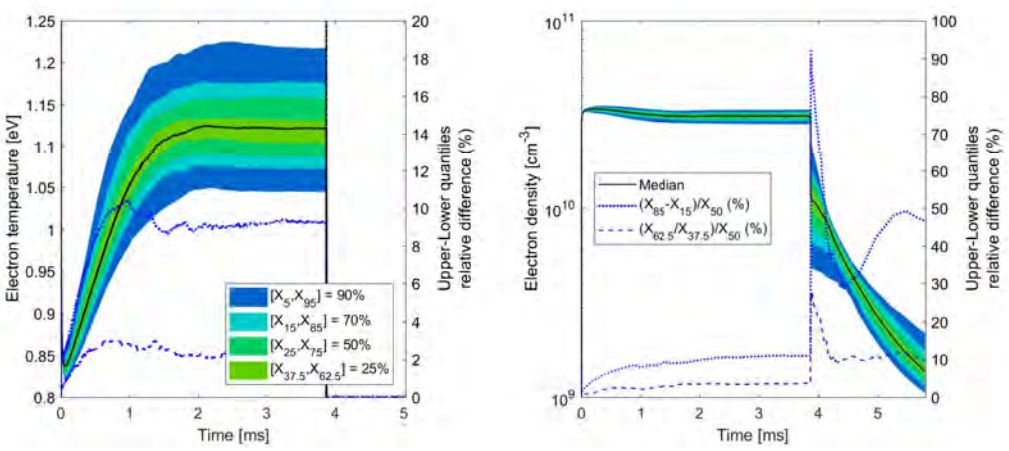

Figure 8. Electron temperature (left panel) and electron density (right panel) as a function of time, calculated by applying a power pulse of nearly 4 ms, until a specific energy input of 1 eV/molecule is obtained, for a CO_2 plasma at 300 K gas temperature, 2×10^4 Pa gas pressure and 200 W cm^{-3} power density. The end of the power pulse is indicated by the vertical dashed black line. The different colors denote different quantiles of 400 solutions, as defined by the uncertainty in the various rate coefficients (see detailed explanation in [124]). The median value is shown by the black curve. The right y-axis gives the relative difference between the upper and lower quantiles, for the confidence interval of 70% (dotted blue line) and 25% (dashed blue line).

When constructing a model, it is tempting to include all possible reactions for all species. However, as the corresponding rate coefficients are often subject to uncertainties, the difficulties in estimating the uncertainty in the calculation results increase with the number of reactions included. This has also been demonstrated by Turner [121, 122], who showed that reaction schemes can be drastically reduced, even up to 85%, without significantly affecting the calculation results [122]. Besides the MC approach presented by Turner, Lehman also proposed an algorithm to identify the

significant pathways [125], which was used to create the software tool PumpKin. The latter allows to identify which processes are important over different time scales [126].

Note that global models are particularly useful also to reduce full reaction schemes into more limited chemistry sets, which can then be applied in the solution of 2D or 3D fluid models [127]. The combination of global models to study the detailed plasma chemistry on the one hand, with 2D/3D fluid models with more limited chemistry sets but with detailed description of the reactor setup on the other hand, can be very powerful, *e.g.* for gas conversion applications [112]. However, the reduced chemistry sets defined in this way must be considered with caution, as the dominant pathways might be highly-dependent on the plasma conditions adopted.

5.3.2. Need for assumptions

Another limitation of global models is that they are not self-consistent, relying on certain assumptions on the input data provided, such as the value of the electric field or the EEDF adopted. At sufficiently high pressure (*e.g.* $\sim 10^5$ Pa), when the LFA holds (see section 4), i.e. when the electrons undergo enough collisions to be considered in equilibrium with the local reduced electric field, the EEDF can be obtained from a Boltzmann solver adopting the homogeneous two-term approximation, such as Bolsig+ [128]. Likewise, at very low pressure (*e.g.* a few Pa) and for highly-ionized plasmas, such as inductively coupled plasmas, a Maxwellian EEDF can be taken. However, in the intermediate pressure range a certain EEDF must be assumed, which might affect the calculation results depending on the quality of the assumption.

5.3.3. Lack of spatial variations, and solutions to overcome this limitation

The major limitation of global models is that they consider the plasma to be uniform or, in the best scenario, they provide a spatially-averaged description of the plasma. Indeed, the above balance equations yield the time-evolution of the species densities, averaged over the volume of the plasma reactor, while spatial variations, *e.g.* due to transport in the plasma, are not considered. Nevertheless, several methods have been proposed in literature to account in global models for the presence of spatially-dependent phenomena, as discussed in detail in [80].

The primary method to introduce the influence of spatial variations into a global model is the use of a factor describing the relationship between the ion density in the centre of the plasma and the ion density at the sheath edge, the so-called h_l factor [80]. Furthermore, the effect of diffusion and losses due to the sticking of species at the walls is often accounted for by adding an extra loss term in the balance equations. This can be done by calculating the outward flux of particles $\Gamma_{i,wall}$, directed to the surface A of the wall, and by adding the term $(A/V)\Gamma_{i,wall}$ as a loss term in (36), where V is the plasma volume. Obtaining $\Gamma_{i,wall}$ requires to know the velocity of the particles near the wall. For the ions and the electrons, this velocity can be taken as the Bohm velocity, in coherence with the development of the space-charge sheath near the wall [129]. Hong *et al* recently developed a global model for ammonia synthesis by plasma catalysis,

accounting for surface reactions at the catalyst surface [130]. The production and the destruction rates due to reactions with this surface are then simply included as an additional gain or loss term, consisting of the rate coefficient multiplied by the density of free sites in the surface.

Finally, a global model can also include spatial effects due to the translation of the time variation of some quantity into its space variation, i.e. as a function of the distance travelled by the gas through the plasma reactor, based on the gas flow rate. This is possible due to the similarity between a batch reactor and a plug flow reactor. Indeed, when the plasma reactor is considered as a plug flow reactor, the temporal variation of a gas-related quantity corresponds to a variation as a function of the gas residence-time in the reactor or, in other words, as a function of the distance in the reactor. In this way, it is possible to account for spatial variations of input power or gas temperature inside the plasma reactor, to be used as input parameters to the global model. This is useful for a plasma jet, expanding in (humid) air. Indeed, by assuming a certain power deposition (and gas temperature) as a function of the distance from the nozzle exit, obtained from experiments, and by accounting for the speed of humid air diffusion within the noble gas stream, a global model can be used in a semi-empirical way to mimic the experimental conditions, as demonstrated in [89].

The same approach can also be applied in reactors used for gas conversion. For instance, in a microwave plasma the power deposition has its maximum value at the position of the waveguide, hence one can assume that the gas temperature will start to increase around this position. This is illustrated in figure 9.

Likewise, the filamentary behaviour of a dielectric barrier discharge (DBD) can be accounted for by applying a number of pulses as a function of time, which represent the microdischarge filaments inside the DBD reactor that the gas molecules would pass when they travel through the reactor. This method is conceptually much easier than accounting for filament formation in a 1D, 2D or 3D fluid model. Details of this approach can be found in [104, 106, 131].

6. Plasma-surface mesoscopic models

The study of plasma-surface interactions is nowadays a very active field of research, prompted by its relevance in applications such as etching and deposition [132–134], volatile organic compound abatement [135–138] and atmospheric re-entry studies [139, 140].

The modelling of plasma-surface interactions is a multi-scale problem. The shortest time-scale is associated with the vibrational motion of molecules and adsorbed species on the surfaces, which takes place in the order of fs. The atomic-scale description of the elementary steps of adsorption, desorption, diffusion, and reactions on the surface comes next. These are often thermally activated processes, occurring in time-scales in the range ns-ms. In turn, real experiments may involve the description of the surface dynamics along seconds or several minutes.

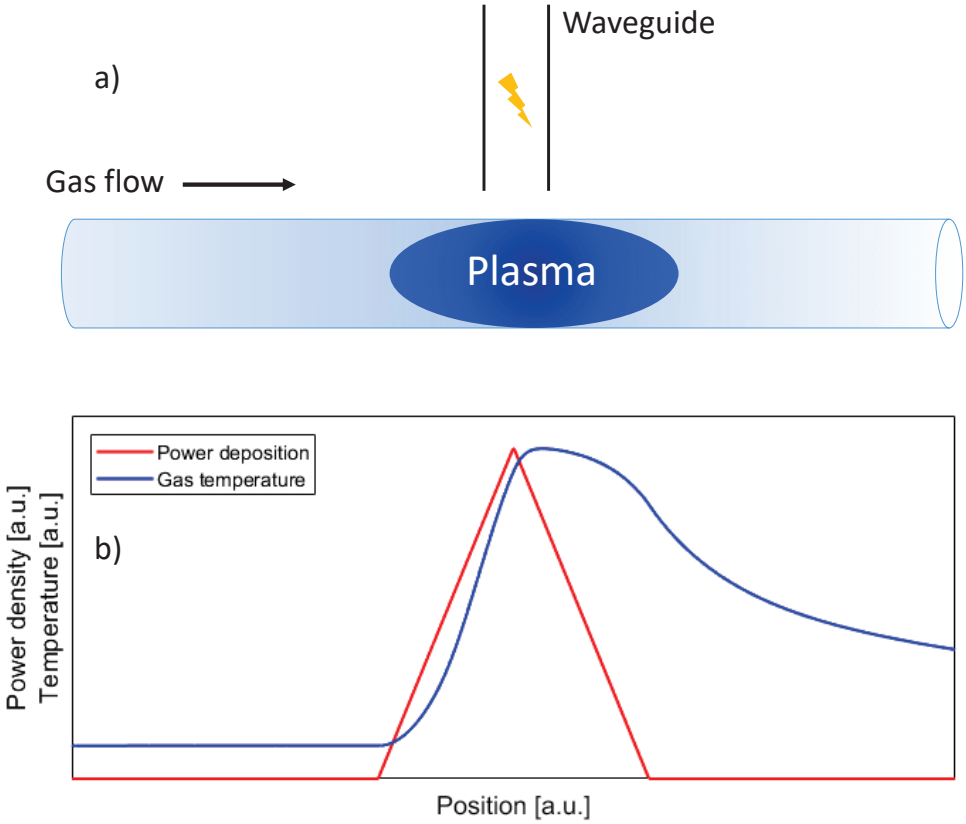

Figure 9. Simplified schematic of a surfatron microwave plasma (a), with power deposition and corresponding gas temperature profile as assumed in the model (b).

One of the most detailed descriptions of surface interactions can in principle be obtained from density functional theory, a fully quantum technique, in which the energy of the system is expressed as a function of the electron density, thus avoiding the difficulty of handling many-body wave-functions. It can be highly accurate, but the size of the systems it can study remains very small, at best accounting for a few hundred atoms. It is usually applied to highly-idealized systems and it does not include any plasma-specific processes [141–143]. Nevertheless, these studies can bring insight into some specific reactions, *e.g.* by calculating the associated energy barriers. Moreover, they can be used to parametrize potential energy surfaces that can be used in classical molecular dynamics simulations.

Classical molecular dynamics computations integrate the equations of motion of all atoms in the system, considering forces derived from a classical interatomic interaction potential, often a potential energy surface obtained from density functional theory. They can treat thousands to millions of atoms and the accessible time-scale of the simulations is of the order of ns [144–147], still far from the time (and length) scales involved in a real system. Another challenge to molecular dynamics calculations is to accurately account for electronically and vibrationally excited states, electromagnetic fields, charged particles and photons. Therefore, the application of classical molecular

dynamics to realistic molecule formation under plasma conditions is still difficult and the coupling of surface interactions with complex gas-phase chemistry remains unfeasible.

A class of *accelerated dynamics* techniques have been recently developed to extend molecular dynamics simulations up to timescales of the order of seconds. The general idea is to assume that the system is most of the time confined to a local minimum of the potential energy surface until some rare fluctuation induces a transition to another local minimum, and to increase the hopping rates between local minima of the potential energy surface. This accelerated dynamics can be achieved by working at higher temperatures [148] – an approach that has the drawback of modifying the dynamics of the system, as the relative rates of the different processes are altered – or by lowering the energy barriers for the transitions between the minima of the potential energy surfaces (hyperdynamics) [149, 150].

An alternative solution to bridge the gap between the detailed atomistic description of the shortest time-scales and the macroscopic scales relevant to study real systems is to develop coarse-grained *mesoscopic models*, which are probably the best tool to model plasma-surface interactions in realistic conditions. These models can adopt either a stochastic or a deterministic description of the system and have been recently reviewed in [151, 152]. They can effectively include an interesting degree of microscopic detail of the surface kinetics, be coupled with gas phase chemistry and be used to describe both the steady-state and the dynamics of the system, without any significant limitation on the reachable time-scales. Mesoscopic models are thus a very suitable tool to describe, interpret and acquire physical insight into the phenomena underlying plasma-surface interactions. However, they lack to some extent a truly predictive power, as they need as input the energy barriers for each elementary step and other physical parameters. Moreover, they typically consider a static surface, not accounting for surface modifications under plasma exposure. This latter aspect can in principle be included in the models without much difficulty from a technical point of view, but the formulation of the physical problem and its validation are not straightforward.

6.1. Formulation of mesoscopic models

The most detailed mesoscopic description can be modelled with Kinetic Monte Carlo (KMC) algorithms, sometimes referred to as dynamic Monte Carlo, whose foundations were established by Daniel Gillespie in the 1970s [153, 154]. These algorithms are exact, simple to implement, can describe the properties of fluctuations and probabilities that may depend on the local configuration of the surface, and provide a good treatment of physisorbed species. KMC methods do not solve explicitly the master equation for a given system, but instead numerically simulate the subjacent Markov process. Hence, the individual surface processes are treated as discrete jumps between the successive states of the system, where the transition to the next state depends exclusively on the current state of the system and does not depend on its past history [151, 152, 155–158].

The master equation can be written as

$$\frac{\partial P(\sigma,t)}{\partial t} = \sum_{\sigma'} \left[W(\sigma' \to \sigma) P(\sigma',t) - W(\sigma \to \sigma') P(\sigma,t) \right] \quad , \tag{40}$$

where $P(\sigma,t)$ is the probability of finding the system in state σ at instant t, σ and σ' are successive states of the system and $W(\sigma \to \sigma')$ is the probability per unit time that the system undergoes a transition from state σ to state σ'. The first term of the sum in the right-hand side represents the increase in $P(\sigma,t)$ because of events responsible for a change of the system into state σ from any other state σ', while the second term is the decrease in $P(\sigma,t)$ due to all events that make the system leaving state σ. Note that the surface is represented as a grid of active sites that can hold atoms and molecules, so that the state of the system can be described as a list of all active sites in the simulation domain and their respective occupancies.

The master equation is often written directly from intuitive arguments, but it can be derived more formally from the Markov chain assumption and the consequent Chapman-Kolmogorov equation for the transition probabilities of a Markov process [159, 160]. In the case of surface kinetics, the Markov chain assumption is valid as long as the simulated events take place on a much longer timescale than the lattice vibrations, so that both timescales become decoupled [158]. In this case, the memory of which states were previously visited is effectively lost due to the vibrations between two transitions near the local minima of the potential energy surface.

KMC simulations are exact in the sense they follow the evolution of one element of the statistical ensemble, simulated without any subjacent approximation, by providing the answers to the questions "when, where and what". In short, it is considered that the system may undergo k transition events,

$$\mathcal{E} = \{e_1, e_2, \cdots, e_k\} \quad , \tag{41}$$

characterised by transition rates

$$\mathcal{R} = \{r_1, r_2, \cdots, r_k\} \quad , \tag{42}$$

while the number of particles capable of experiencing a given event is divided as

$$\mathcal{N} = \{n_1, n_2, \cdots, n_k\} \quad . \tag{43}$$

Upon the successful choice of "what" and "where", time is advanced by randomly selecting an increment τ from an exponential distribution with parameter

$$\lambda = \sum_i n_i r_i = \sum_i \lambda_i \quad , \tag{44}$$

namely

$$\tau = \frac{1}{\lambda} \ln\left(\frac{1}{r}\right) \quad , \tag{45}$$

where r is a random number drawn from the uniform distribution in the unit interval, as initially proposed in [161]. The choice of the event type is made by drawing a uniform random number between 0 and λ (*cf.* (44)) and verifying to which interval

$[0, \lambda_1), [\lambda_1, \lambda_1 + \lambda_2), \cdots$ it corresponds. Expression (45) ensures that dynamical MC methods provide an accurate treatment of time, with the desired correspondence between MC time and real time [153, 162].

There are several ways to implement the procedure described above. Two of the most common are the so-called null-event algorithms and the n-fold way or BKL (Bortz-Kalos-Lebowitz) algorithm. These methods have been recently presented and carefully discussed in [151, 152]. Their main difference is in the order of acquiring the answers to the questions "where" and "what". In [151, 152] it was pointed out that the BKL formulation is far superior to study surface kinetics, since the transition rates of the different elementary processes can vary over ~ 10 orders of magnitude. It first answers the question "what", *i.e.* which type of event e_j will happen next, and only then the question "where", by choosing the site on the surface where it will happen from a list of possible sites for e_j.

Efficient algorithms describing NO and O_2 recombination in silica were recently presented [151, 152] opening the door for a significant development of this approach. In particular, a new variant of the BKL algorithm was proposed in [151], denoted as BKL*, where the choice of an empty physisorption site was made with a null-event scheme and no list of empty physisorption sites was kept. The primary reason for this choice is that, for these systems and typical operating conditions, the vast majority of sites on the surface are indeed empty physisorption sites, all along the simulation (the fractional coverage of physisorption sites is in the range $10^{-7} - 10^{-4}$). Handling a huge list of empty physisorption sites turned out to be computationally expensive and a gain in computation time up to 20% was attained.

In order to reduce the statistical fluctuations in the simulations, it is possible to increase the number of surface sites considered in a single simulation or to average the results over several realisations of the system. The latter procedure corresponds to follow different points of the statistical ensemble and is formally more appealing. In fact this averaging procedure should be performed even if the number of surface sites is large enough to ensure smooth dependencies of the different quantities on a single run. As it has been shown in [151] for the case of NO oxidation on silica and is presented in section 6.2, the total CPU time used to achieve similar results using either procedures is very similar. Therefore, averaging over several simulations can be more interesting from the computational point of view, as different runs can be launched simultaneously on different computer cores, leading to a significant gain in real computation time.

A different class of mesoscopic models adopts a deterministic description (DD) of the dynamics of the system, formulated in terms of average fractional coverages of different types of adsorption sites, as initially proposed by Kim and Boudart [163]. The time-evolution of the adsorbed species and adsorption sites is then ruled by a system of reaction-rate differential equations associated with the different elementary processes taken into account, similar to the balance equations (36) of gas-phase global models [163–167]. The main advantage of this approach is its simplicity and computational efficiency, which allows the straightforward coupling to gas phase

chemistry in reactor-scale simulations and in computational fluid dynamics codes. However, compared to KMC, it does not account for spatial correlations and cannot handle easily probabilities that depend on the local configuration of the system, cannot characterize fluctuations (and in fact fails when the fluctuations in the number of particles are important), relies on additional assumptions regarding the treatment of physisorbed species [151, 152] and is not suited to handle systems with distributions of reactivity or binding energies among the adsorption sites [152].

6.2. Examples

As an illustration of the power and interest of mesoscopic surface models, we present a few results taken from [151, 152, 168], regarding NO oxidation on pre-treated Pyrex and oxygen recombination on silica.

NO oxidation with O atoms previous adsorbed on a Pyrex wall was investigated by Guaitella and co-workers, in a series of experiments dedicated to the study of surface kinetics [169, 170]. Basically, an oxygen discharge is run on a Pyrex tube of radius 1 cm and length 60 cm for about 1 h. The discharge tube is then pumped out to let the system cool down and remove any gas phase and short lived adsorbed species. Finally, an injection of $0.1 - 4$ Torr ($\sim 10 - 500$ Pa) of NO diluted in argon is made in the closed tube and the kinetics of both NO and NO_2 is measured using a diode laser spectrometer.

The model assumes a surfaced covered with 7 types of chemisorption sites, corresponding to different activation energies for recombination, in the range $16 - 41$ kJ/mol, which hold the previously grafted oxygen atoms. NO oxidation takes place in reactions

$$NO + O_S(i) \rightarrow NO_2 + S_V(i) \quad , \tag{46}$$

where NO and NO_2 represent gas-phase molecules, $O_S(i)$ represents a chemisorbed oxygen atom on a site of type i, and $S_V(i)$ represents an empty chemisorption site of type i. A slow loss of N-containing molecules is accounted for, assuming a slow adsorption of NO_2 molecules that can be schematically represented as

$$NO_2 + S_V(i) \rightarrow (NO_2)_S \quad , \tag{47}$$

where $(NO_2)_S$ represents an adsorbed NO_2 molecule. Notice that this system effectively corresponds to a description of coupled gas-phase and surface-kinetics.

The results are shown in figure 10, which compares the calculations from KMC (full curves) and DD (dashed curves) simulations. The excellent agreement between the results of both simulations is immediately evident. A comparison with the experimental data can be found in [168], revealing a very good agreement between the modelling results and the measurements. The very different time-scales for NO_2 formation when the pressure varies from 0.1 to 4 Torr are a manifestation of a distribution of reactivity among different adsorption sites, attributed to different bond strengths of adsorbed O atoms with the surface [151].

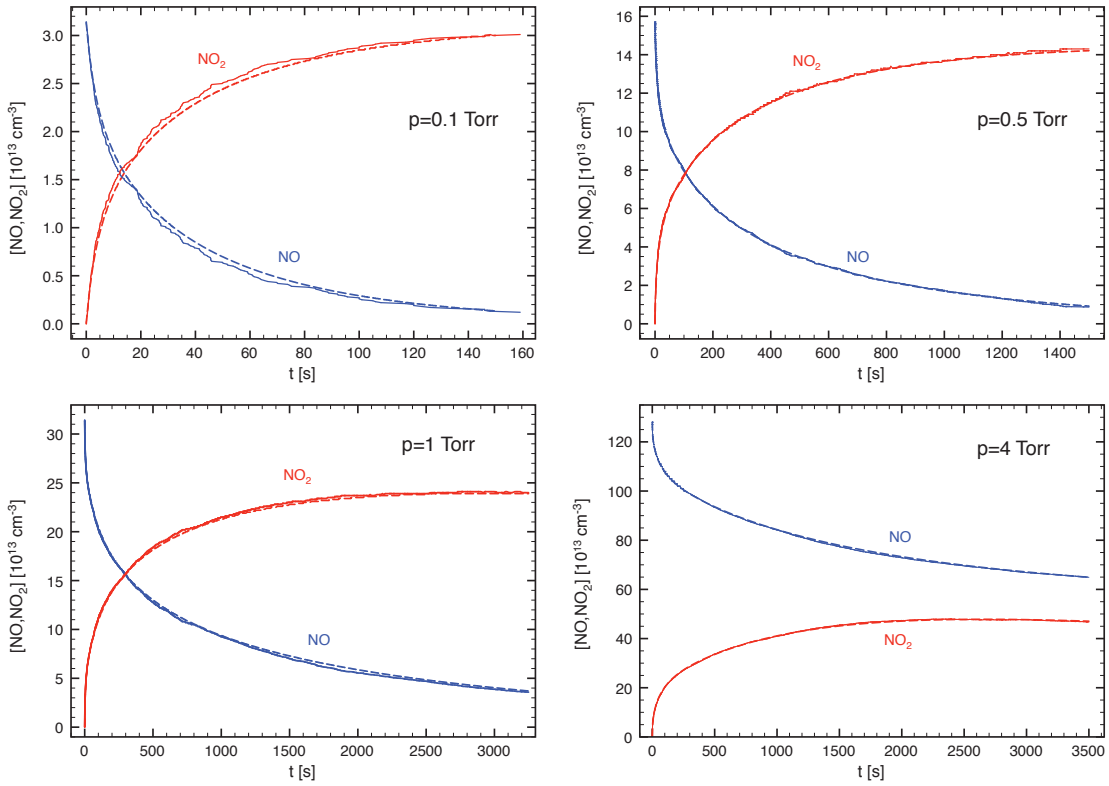

Figure 10. Calculated time-evolution of the gas-phase concentrations of NO (blue curves) and NO_2 (red) from a KMC (—) and DD (– –) model, for various pressures. Taken from [151].

Figure 11 shows the evolution of the error associated with the calculation of the NO concentration as a function of the used CPU time, when increasing the number of sites on the grid and the number of realisations of the system included in the averaging procedure for grids with constant number of points, for two values of the pressure. This error is calculated from the dispersion of the random variable $[\mathrm{NO}]_{KMC}(t_i)$-$[\mathrm{NO}]_{DD}(t_i)$, defined as

$$\Delta = \sqrt{\sum_{i=1}^{N} \left([NO]_{KMC}(t_i) - [NO]_{DD}(t_i)\right)^2} \quad , \tag{48}$$

where $[\mathrm{NO}]_{KMC}(t_i)$ and $[\mathrm{NO}]_D(t_i)$ are the single run concentrations of NO molecules at instants t_i obtained by KMC and DD simulations, respectively, which has an expectation value of zero. The absolute error is then calculated by the average value of Δ on 50 KMC runs (see [151] for details). This figure illustrates the decrease of the statistical fluctuations of the KMC calculations by different procedures and confirms that, for the system under analysis, the total CPU time to achieve one specific value of the error is nearly constant regardless of the strategy followed.

The second illustration of surface modelling regards oxygen recombination on silica

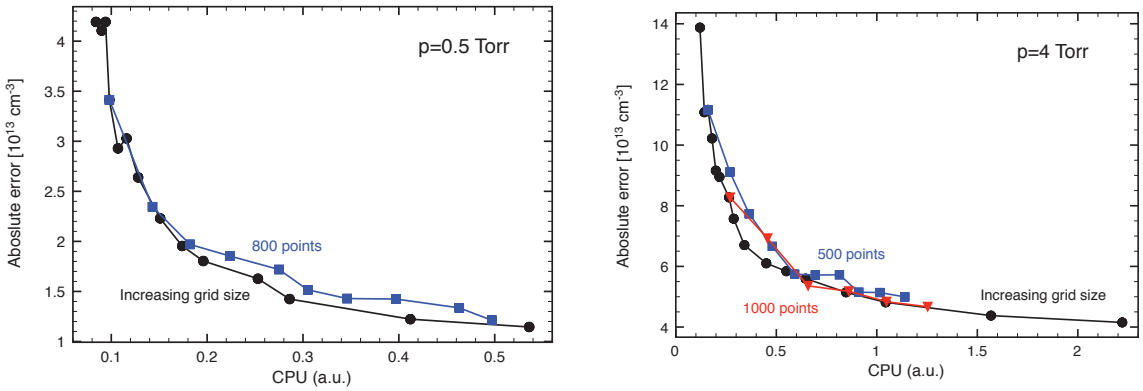

Figure 11. Error associated with the calculation of [NO] as a function of the used CPU time, when increasing the number of sites on the grid (black curves) and the number of realisations of the system included in the averaging procedure for grids with constant number of points (blue and red), for various pressures. Taken from [151].

according to [151, 152, 166]. The following elementary processes are taken into account: physisorption; thermal desorption from physisorption sites; chemisorption; Eley-Rideal recombination; surface diffusion of physisorbed atoms; and Langmuir-Hinshelwood recombination. These can be represented by the set of reactions

$$O + F_V \rightarrow O_F \tag{49a}$$
$$O_F \rightarrow O + F_V \tag{49b}$$
$$O + S_V \rightarrow O_S \tag{49c}$$
$$O + O_S \rightarrow O_2 + S_V \tag{49d}$$
$$O_F + S_V \rightarrow F_V + O_S \tag{49e}$$
$$O_F + O_S \rightarrow O_2 + F_V + S_V \tag{49f}$$
$$O_F + O_F \rightarrow O_2 + F_V + F_V \tag{49g}$$

where O and O_2 are gas phase atoms and molecules, F_V and S_V are empty physisorption and chemisorption sites, respectively, and O_F and O_S and physisorbed and chemisorbed atoms.

In this scheme, the main differences between KMC and DD simulations arise from the treatment of processes (49*e*)-(49*g*) involving diffusing physisorbed atoms. As carefully discussed in [151, 152], these mechanisms are rigorously described in the KMC approach, which directly accounts for the random walk motion of a diffusing physisorption atom on the surface. In turn, the inclusion of these mechanisms in DD models involves the calculation of approximate expressions considering an average global rate, which is the outcome of a sequence of elementary steps [152, 163, 166].

The recombination probabilities calculated from the mechanisms (49*a*)-(49*g*) and appropriate surface parameters are in very good agreement with experimentally obtained data (see [151, 152, 166] for details and information on surface parameters). Here, we focus on differences between the results of KMC and DD simulations. Figure 12 shows

the time evolution of the fractional coverage of physisorption sites, θ_F, for two values of the wall temperature, $T_W = 300, 200$ K. The steady-state values are of the order of 10^{-6} and 10^{-3}, respectively. They are higher for the lower temperature, as a result of less efficient thermal desorption. Inspection of the figure reveals that for $T_W = 300$ K

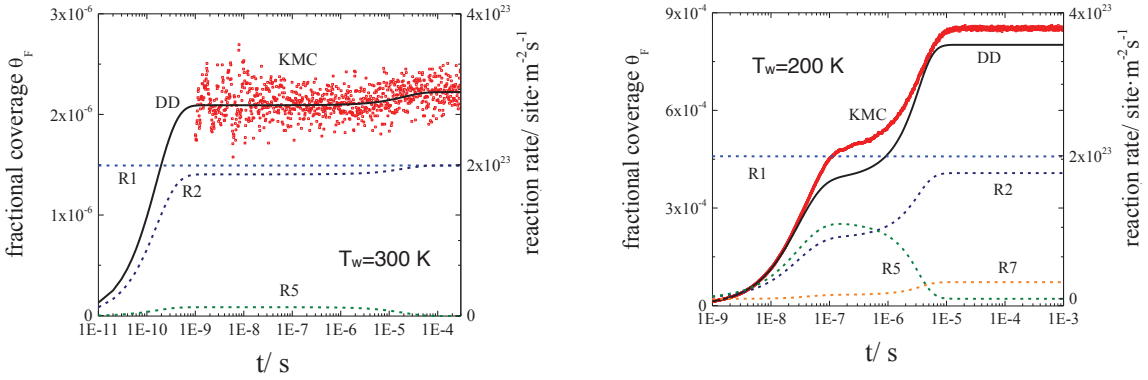

Figure 12. Time evolution of the fractional coverage of physisorption sites and rates, for wall temperatures $T_W = 300, 200$ K and the following mechanisms: R_1 (49*a*); R_2 (49*b*); R_5 (49*e*); R_7 (49*g*). Taken from [152]. Copyright Wiley-VCH Verlag GmbH & Co. KGaA. Reproduced with permission.

the approximations used in the calculation of the rate coefficients of processes (49*e*)-(49*g*) in the deterministic model provide very good results, both for the dynamics and the steady-state values of θ_F. For $T_W = 200$ K, however, the fractional coverage of physisorption sites is already high enough to cause some differences between the KMC and DD calculations, indicating limitations in the validity of these approximations.

7. Final remarks and outlook

Modelling and simulation activities in the field of LTPs are an essential and widely embraced research component for investigating fundamental processes, providing quantitative predictions on the behaviour of systems, guiding the design of experiments and diagnostics, and optimizing devices. Additionally, the number of researchers dedicated to these activities has also increased, following a broad use of modelling and simulation tools largely driven by applications and facilitated by the access to commercial codes.

This paper was dedicated to presenting the basis of some of the most common plasma models (PIC with MC collisions, kinetic equation, fluid, global and plasma-surface), providing key information for a beginner in the field to get acquainted with the advantages and limitations of each approach. The paper is intended merely to serve as entry point for acquiring basic knowledge in modelling and simulation, contributing also to motivate students and researchers for the importance of these activities in LTPs. A more in-depth training in the subject requires a thorough reading of many books and papers from the extensive list of references proposed. Also, the paper presents very

different plasma models, in terms of the approaches adopted and the results provided, that should be selected according to the goals intended and the systems under study. Indeed, the choice of the "best plasma model" for each research program depends on (i) the specific information about the system (dimensions, gas pressure and temperature, excitation conditions); (ii) the goals of the study (which quantities to calculate and for what purpose); (iii) the transport features (suggested by the values of the Debye length and the typical mean-free-paths); (iv) the kinetic features (depending on the current knowledge of the reaction scheme for the gas-mixture of interest, and considering the level of detail intended for the study).

PIC simulation with MC collisions are an appropriate choice if one intends to capture phase space distributions in the most general way, and couple particle motions with the fields essentially without approximation. Consequently, studies with PIC simulations are often valuable when addressing fundamental physics questions. Moreover, computationally less expensive approaches, such as fluid or global models, depend for their validity on assumptions that are difficult to verify in many physical situations. PIC simulations may be used to explore the applicability of such assumptions.

Kinetic equation models are real alternative to PIC simulations, particularly if the focus is on obtaining the energy distribution for electrons, without the need for a spatial description of the plasma. The two-term approximation, consisting in a spherical harmonics development to the second order in velocity space of the electron distribution function, is the most popular approach for solving the EBE, calculating the EEDF, and obtaining the corresponding electron transport parameters and rate coefficients.

Fluid models are extremely competitive (in terms of both the simplicity of the formulation and the computational resources required), in cases where the space-time description of the plasma is important, while one can accept to lose some insight on the energy distribution of species, as well as to adopt a reduced (simpler) reaction scheme. These limitations can be partially circumvented by using hybrid approaches, *e.g.* combining fluid simulations with a kinetic description for electrons (adopting either the LFA or the LEA) and a collisional-radiative (global) model for the gas/plasma chemistry. Indeed, only rarely is there both technical justification and sufficient resources to pursue a fully kinetic investigation of a chemically and geometrically physical complex system, so usually a fluid or hybrid model is the preferred solution in such cases.

When the focus is on the chemistry of the system, global models are probably the best option. They are based on solving simple (particle and energy) balance equations based on (a large number of) chemical reactions. They are easy to program and don't require large computational effort. Global models are very useful for chemical reaction pathway analysis, to study the most important production and loss processes for various species. This provides insight in the limitations for the production of some species, so that solutions can be proposed on how to overcome these limitations. On the other hand, the fact that global models usually describe a detailed plasma chemistry also indicates their main weakness, *i.e.* the need for accurate reaction rate coefficients. The

latter are often subject to uncertainties, and this limits the predictive character of the global modelling results. Furthermore, the major limitation of global models is that they provide a spatially-averaged description of the plasma, although several methods have been proposed to take into account spatially-dependent phenomena.

Mesoscopic plasma-surface models, adopting either KMC or DD approaches, are at present the best available tool to simulate and investigate surface kinetics up to relevant macroscopic time-scales, as well as to describe and study coupled gas phase and surface chemistries. There is still a gap between the sophistication of molecular dynamics and the effectiveness and simplicity of mesoscopic deterministic models, and this is probably the most pressing challenge on the modelling of surface kinetics. KMC simulations can play a key role in bridging this gap: they can incorporate the information coming from molecular dynamics regarding binding energies, energy barriers and dynamic surface modifications; and they can also be used to validate and benchmark DD models and the underlying approximations.

Regardless of the specific plasma model chosen, the research work that follows will imply using a numerical code and sets of elementary data as input parameter. The code should be adequately *verified*, namely to minimize programming bugs, to ensure they preserve basic conservation laws and to certify they provide expected physical solutions in known limiting cases. These cautions must be taken for both commercial and in-house codes, and for the latter collaborative efforts leading to open-source tools are a viable solution with increasing acceptance. The data should also be critically assessed, instead of just collected from the different references and databases available. In some cases, the uncertainties in the elementary data adopted can lead to orders of magnitude differences in the results obtained, thus limiting considerably the interest of modelling and simulation activities.

Finally, one should never overlook the enormous potential of modelling and simulation as a predictive tool. However, this goal can only be achieved after a *validation* process, by comparing modelling results with experimental measurements. Again, this step requires a great deal of collaborative work, this time involving experimental teams, whose contribution is paramount for the proper development of codes and the successful implementation of modelling and simulation research programs.

Acknowledgments

The authors would like to thank A Tejero-Del-Caz and A Berthelot for their technical contributions in writing the manuscript. This work was partially funded by Portuguese FCT - Fundação para a Ciência e a Tecnologia, under projects UID/FIS/50010/2013, PTDC/FISPLA/1243/2014 (KIT-PLASMEBA) and PTDC/FIS-PLA/1420/2014 (PREMiERE).

References

[1] Adamovich I, Baalrud S D, Bogaerts A, Bruggeman P J, Cappelli M, Colombo V, Czarnetzki U, Ebert U, Eden J G, Favia P, Graves D B, Hamaguchi S, Hieftje G, Hori M, Kaganovich I D, Kortshagen U, Kushner M J, Mason N J, Mazouffre S, Mededovic Thagard S, Metelmann H-R, Mizuno A, Moreau E, Murphy A B, Niemira B A, Oehrlein G S, Petrovic Z Lj, Pitchford L C, Pu Y-K, Rauf S, Sakai O, Samukawa S, Starikovskaia S, Tennyson J, Terashima K, Turner M M, van de Sanden M C M and Vardelle A 2017 *J. Phys. D: Appl. Phys.* **50** 323001

[2] National Research Council of the National Academics 2007 *Plasma Science: Advancing Knowledge in the National Interest* (Washington, DC: National Academies Press)

[3] *The International Technology Roadmap for Semiconductors* 2015

[4] Murphy A B and Uhrlandt D 2017 *Plasma Sources Sci. Technol.* , to be submitted

[5] Shkarofsky I P, Johnston T W and Bachynski M P 1966 *The Particle Kinetics of Plasmas* (Massachusetts, Reading: Addison-Wesley)

[6] Birdsall C K and Langdon A B 1985 *Plasma Physics via Computer Simulation* (New York: McGraw-Hill)

[7] Hockney R W and Eastwood J W 1988 *Computer Simulation using Particles* (Bristol: Adam Hilger)

[8] Birdsall C K 1991 *IEEE Transactions on Plasma Science* **19** 65-85

[9] von Keudell A and Schulz-von der Gathen V 2017 *Plasma Sources Sci. Technol.* **26** 113001

[10] Vahedi V and Surendra M 1995 *Comput. Phys. Commun.* **87** 179-198

[11] Donkó Z 2011 *Plasma Sources Sci. Technol.* **20** 024001

[12] Skullerud H R 1969 *J. Phys. B: At. Mol. Phys.* **2** 696-705

[13] Bird G A 1994 *Molecular Gas Dynamics and the Direct Simulation of Gas Flows*, *Oxford Engineering Science Series* vol. 42 (Oxford: Oxford University Press)

[14] Boyd I D 1996 *Journal of Thermophysics and Heat Transfer* **10** 579-585

[15] Turner M M, Derzsi A, Donkó Z, Eremin D, Kelly S J, Lafleur T and Mussenbrock T 2013 *Physics of Plasmas* **20** 013507

[16] Turner M M and Hopkins M B 1992 *Phys. Rev. Lett.* **69** 3511-3514

[17] Croes V, Lafleur T, Bonaventura Z, Bourdon A and Chabert P 2017 *Plasma Sources Sci. Technol.* **26** 034001

[18] Decyk V and Singh T V 2015 *Comp. Phys. Comm.* **185** 708-719

[19] Meierbachtol C S, Collin S, Greenwood A D, Verboncoeur J P and Shanker B 2015 *IEEE Trans. Plasma Sci.* **43** 3778-3793

[20] Turner M M 2016 *Plasma Sources Sci. Technol.* **25** 054007

[21] Riva F, Beadle C F and Ricci P 2017 *Physics of Plasmas* **24** 055703

[22] Chapman S and Cowling T G 1939 *The Mathematical Theory of Non-uniform Gases* (Cambridge: Cambridge University Press)

[23] Huang K 1963 *Statistical Mechanics* (New York: Wiley)

[24] Nicholson D R 1983 *Introduction to Plasma Theory* (New York: Wiley)

[25] Allis W P 1956 *Motions of ions and electrons* in *Handbuck der Physik* vol. 21 (S Flügge, Berlin: Springer) 383-444

[26] Loureiro J and Amorim J 2016 *Kinetics and Spectroscopy of Low Temperature Plasmas* (Switzerland: Springer)

[27] Bittencourt J A 2004 *Fundamentals of Plasma Physics* (New York: Springer)

[28] Kushner M J 2009 *J. Phys. D: Appl. Phys.* **42** 194013

[29] van Dijk J, Kroesen G M W and Bogaerts A 2009 *J. Phys. D: Appl. Phys.* **42** 190301

[30] White R D, Robson R E, Dujko S, Nicoletopoulos P and Li B 2009 *J. Phys. D: Appl. Phys.* **42** 194001

[31] Lorentz H A 1905 *The motion of electrons in metallic bodies I* in *proceedings Royal Netherlands Academy of Arts and Sciences (KNAW)* vol. 7 (Amsterdam: KNAW) 438-453

[32] Holstein T 1946 *Phys. Rev.* **70** 367-384
[33] Delcroix J-L 1963, 1966 *Physique des Plasmas volumes 1 et 2* in *Monographies Dunod* (Paris: Dunod) (in French)
[34] Braglia G L, Wilhelm J and Winkler E 1985 *Lett. Nuovo Cimento* **44** 365-378
[35] Phelps A V and Pitchford L C 1985 *Phys. Rev.* A **31** 2932-2949
[36] Petrov G and Winkler R 1997 *J. Phys. D: Appl. Phys.* **30** 53-66
[37] Blevin H A and Fletcher J 1984 *Aust. J. Phys.* **37** 593-600
[38] Winkler R, Wilhelm J and Braglia G L 1986 *Nuovo Cimento D* **7** 641-680
[39] Kumar K, Skullerud H R and Robson R E 1980 *Aust. J. Phys.* **33** 343-448
[40] Segur P, Bordage M-C, Balaguer J-P and Yousfi M *J. Comput. Phys.* **50** 116-137
[41] Frost L S and Phelps A V 1962 *Phys. Rev.* A **127** 1621-1633
[42] Huxley L G H and Crompton R W 1974 *The Diffusion and Drift of Electrons in Gases* Ch. 13 (New York: John Wiley &)
[43] Petrović Z Lj , Dujko S, Marić D, Malović G, Nikitovic Z, Sasić O, Jovanović J, Stojanivić V and Radmilović-Radenović M 2009 *J. Phys. D: Appl. Phys.* **42** 194002
[44] Ferreira C M and Loureiro J 2000 *Plasma Sources Sci. Technol.* **9** 528-540
[45] Shkarofsky I, Johnston T and Bachynski M 1966 *The Particle Kinetics of Plasmas* (Addison-Wesley Publishing Company)
[46] Ridenti M A, Alves L L, Guerra V and Amorim J 2015 *Plasma Sources Sci. Technol.* **24** 035002
[47] Yoshida S, Phelps A V and Pitchford L C 1983 *Phys. Rev.* A **27** 2858-2867
[48] Yousfi M, Ségur P and Vassiliadis T 1985 *J. Phys. D: Appl. Phys.* **18** 359-375
[49] Itoh H, Miura Y, Ikuta N, Nakao Y and Tagashira H 1988 *J. Phys. D: Appl. Phys.* **21** 922-930
[50] Tejero-del-Caz A, Nina D, Jacob S, Gonçalves D, Lino da Silva M, Marques L, Pinhão N R, Pintassilgo C D, Guerra V and Alves L L, *Proceedings XXXIII International Conference on Phenomena in Ionized Gases* (ICPIG) (Tejero Del Caz A and Alves L L eds.), Estoril, Portugal, July 2017, p. 274
[51] IST-Lisbon database www.lxcat.net, retrieved on August 2017
[52] Alves L L 2014 *Journal of Physics: Conference Series* **565** 012007 (and references therein)
[53] Loureiro J and Ferreira C M 1986 *J. Phys. D: Appl. Phys.* **19** 17-35
[54] Loureiro J and Ferreira C M 1989 *J. Phys. D: Appl. Phys.* **22** 67-75
[55] Rose D J and Brown S C 1955 *Phys. Rev.* **98** 310-316
[56] Bernstein I B and Holstein T 1954 *Phys. Rev.* **94** 1475-1482
[57] Tsendin L D 1974 *Sov. Phys. JETP* **39** 805-810
[58] Ingold J H 1997 *Phys. Rev.* E **56** 5932-5944
[59] Busch C and Kortshagen U 1995 *Phys. Rev.* E **51** 280-288
[60] Uhrlandt D and Winkler R 1996 *J. Phys. D: Appl. Phys.* **29** 115-120
[61] Alves L L 2007 *Plasma Sources Sci. Technol.* **16** 557-569
[62] Meijer P M, Goedheer W J and Passchier J D P 1992 *Phys. Rev.* A **45** 1098-1102
[63] Schottky W 1924 *Phys. Z.* **25** 635-645
[64] Tonks L and Langmuir I 1929 *Phys. Rev.* **34** 876-922
[65] Self S A and Ewald H N 1966 *Phys. Fluids* **9** 2486-2492
[66] Ferreira C M and Ricard A 1983 *J. Appl. Phys.* **54** 2261-2271
[67] Forrest J R and Franklin R N 1968 *J. Phys. D: Appl. Phys.* **1** 1357-1368
[68] Ingold J H 1972 *Phys. Fluids* **15** 75-85
[69] Metze A, Ernie D W and Oskam H J 1989 *Phys. Rev.* A **39** 4117-4124
[70] Salabas A, Gousset G and Alves L L 2002 *Plasma Sources Sci. Technol.* **11** 448-465
[71] Alves L L, Gousset G and Vallée S 2003 *IEEE Trans. Plasma Sci.* **31** 572-586
[72] Boeuf J P 1987 *Phys. Rev.* A **36** 2782-2792
[73] Kaneda T 1979 *J. Phys. D: Appl. Phys.* **12** 61-70
[74] Marques L, Jolly J and Alves L L 2007 *J. Appl. Phys.* **102** 063305
[75] Pancheshnyi S, Eismann B, Hagelaar G J M and Pitchford L C 2008, Computer code ZDPlasKin,

http://www.zdplaskin.laplace.univ-tlse.fr
[76] Dorai R and Kushner M J 2003 *J. Phys. D: Appl. Phys.* **36** 1075-1083
[77] Stafford D S and Kushner M J 2004 *J. Appl. Phys.* **96** 2451-2465
[78] Munro J J and Tennyson J 2008 *J. Vac. Sci. Technol.* A **26** 865-869
[79] van Dijk J, Peerenboom K, Jimenez M, Mihailova D and van der Mullen J 2009 *J. Phys. D: Appl. Phys.* **42** 194012
[80] Hurlbatt A, Gibson A R, Schröter S, Bredin J, Foote A P S, Grondein P, O'Connell D and Gans T 2017 *Plasma Process. Polym.* **14** 1600138
[81] Kogelschatz U, Eliasson B and Hirth M 1988 **Ozone Sci. Eng. 10** 367-377
[82] Kossyi I A, Kostinsky A Y, Matveyev A A and Silakov V P 1992 *Plasma Sources Sci. Technol.* **1** 207-308
[83] Gentile A C and Kushner M J 1995 *J. Appl. Phys.* **78** 2074-2085
[84] Sakiyama Y, Graves D B, Chang H W, Shimizu T and Morfill G E 2012 *J. Phys. D: Appl. Phys.* **45** 425201
[85] Liu D X, Bruggeman P, Iza F, Rong M Z and Kong M G 2010 *Plasma Sources Sci. Technol.* **19** 025018
[86] Waskoenig J, Niemi K, Knake N, Graham L M, Reuter S, Schulz-von der Gathen V and Gans T 2010 *Plasma Sources Sci. Technol.* **19** 045018
[87] Murakami T, Niemi K, Gans T, O'Connell D and Graham W G 2014 *Plasma Sources Sci. Technol.* **23** 025005
[88] Murakami T, Niemi K, Gans T, O'Connell D and Graham W G 2013 *Plasma Sources Sci. Technol.* **22** 015003
[89] Van Gaens W and Bogaerts A 2013 *J. Phys. D: Appl. Phys.* **46** 275201
[90] Van Gaens W and Bogaerts A 2014 *Plasma Sources Sci. Technol.* **23** 035015
[91] Van Gaens W, Bruggeman P J and Bogaerts A 2014 *New J. Phys.* **16** 063054
[92] Van Gaens W, Iséni S, Schmidt-Bleker A, Weltmann K-D, Reuter S and Bogaerts A 2015 *New J. Phys.* **17** 033003
[93] Schmidt-Bleker A, Winter J, Iséni S, Dünnbier M, Weltmann K D and Reuter S 2014 *J. Phys. D: Appl. Phys.* **47** 145201
[94] van Gils C A J, Hofmann S, Boekema B K H L, Brandenburg R and Bruggeman P J 2013 *J. Phys. D: Appl. Phys.* **46** 175203
[95] Hamaguchi S, Ikuse K and Kanazawa T 2014 *JPS Conf. Proc.* **1** 015055
[96] Lietz A M and Kushner M J 2016 *J. Phys. D: Appl. Phys.* **49** 425204
[97] Liu Z C, Guo L, Liu D X, Rong M Z, Chen H L and Kong M G 2017 *Plasma Process. Polym.* **14** (in press)
[98] Zhou L M, Xue B, Kogelschatz U and Eliasson B 1998 *Plasma Chem. Plasma Process.* **18** 375-393
[99] Yang Y 2003 *Plasma Chem. Plasma Process.* **23** 327-346
[100] Nair S A, Nozaki T and Okazaki K 2007 *Chem. Eng. J.* **132** 85-95
[101] Indarto A, Coowanitwong N, Choi J-W, Lee H and Song H K 2008 *Fuel Process. Technol.* **89** 214-219
[102] Goujard V, Nozaki T, Yuzawa S, Ağiral A and Okazaki K 2011 *J. Phys. D: Appl. Phys.* **44** 274011
[103] Agiral A, Nozaki T, Nakase M, Yuzawa S, Okazaki K and Gardeniers J G E 2011 *Chem. Eng. J.* **167** 560-566
[104] Aerts R, Martens T and Bogaerts A 2012 *J. Phys. Chem.* C **116** 23257-23273
[105] Kozák T and Bogaerts A 2014 *Plasma Sources Sci. Technol.* **23** 045004
[106] Snoeckx R, Aerts R, Tu X and Bogaerts A 2013 *J. Phys. Chem.* C **117** 4957-4970
[107] Janeco A, Pinhão N R and Guerra V 2015 *J. Phys. Chem.* C **119** 109-120
[108] Heijkers S, Snoeckx R, Kozák T, Silva T, Godfroid T, Britun N, Snyders R and Bogaerts A 2015 *J. Phys. Chem.* C **119** 12815-12828
[109] Snoeckx R, Heijkers S, Van Wesenbeeck K, Lenaerts S and Bogaerts A 2016 *Energy & Environm. Sci.* **9** 999-1011

[110] Snoeckx R, Ozkan A, Reniers R and Bogaerts A 2017 *ChemSusChem.* **10** 409-424
[111] Bogaerts A, De Bie C, Snoeckx R and Kozák T 2017 *Plasma Process. Polym.* **14** 1600070
[112] Bogaerts A, Berthelot A, Heijkers S, Kolev St, Snoeckx R, Sun S, Trenchev G, Van Laer K and Wang W 2017 *Plasma Sources Sci. Technol.* **26** 063001
[113] Chabert P, Arancibia Monreal J, Bredin J, Popelier L and Aanesland A 2012 *Phys. Plasmas* **19** 073512
[114] Grondein P, Lafleur T, Chabert P and Aanesland A 2016 *Phys. Plasmas* **23** 033514
[115] Raadu M A, Axnas I, Gudmundsson J T, Huo C and Brenning N 2011 *Plasma Sources Sci. Technol.* **20** 065007
[116] Huo C, Lundin D, Raadu M A, Anders A, Gudmundsson J T and Brenning N 2014 *Plasma Sources Sci. Technol.* **23** 025017
[117] Lieberman M A, Lichtenberg A J and Marakhtanov A M 1999 *Appl. Phys. Lett.* **75** 3617-3619
[118] Despiau-Pujo E and Chabert P 2009 *Plasma Sources Sci. Technol.* **18** 045028
[119] Chabert P, Lichtenberg A J, Lieberman M A and Marakhtanov A M 2001 *Plasma Sources Sci. Technol.* **10** 478-489
[120] Corr C S, Steen P G and Graham W G 2003 *Plasma Sources Sci. Technol.* **12** 265-272
[121] Turner M M 2015 *Plasma Sources Sci. Technol.* **24** 035027
[122] Turner M M 2016 *Plasma Sources Sci. Technol.* **25** 015003
[123] Turner M M 2017 *Plasma Sources Sci. Technol.* **14** 1600121
[124] Berthelot A and Bogaerts A *Plasma Sources Sci. Technol.* (in press) DOI: 10.1088/1361-6595/aa8ffb
[125] Lehmann R 2004 *J. Atmos. Chem.* **47** 45-78
[126] Markosyan A H, Luque A, Gordillo-Vazquez F J and Ebert U 2014 *Comput. Phys. Commun.* **185** 2697-2702
[127] Berthelot A and Bogaerts A 2016 *Plasma Sources Sci. Technol.* **25** 045022
[128] Hagelaar G J M and Pitchford L C 2005 *Plasma Sources Sci. Technol.* **14** 722-733
[129] Lieberman M A and Lichtenberg A J 2005 *Principles of Plasma Discharges and Material Processing* 2nd edition (Hoboken, NJ: Wiley-Interscience)
[130] Hong J, Pancheshnyi S, Tam E, Lowke J J, Prawer S and Murphy A B 2017 *J. Phys. D: Appl. Phys.* **50** 154005
[131] Bogaerts A, Wang W, Berthelot A and Guerra V 2016 *Plasma Sources Sci. Technol.* **25** 055016
[132] Hody V, Belmonte T, Pintassilgo C D, Poncin-Epaillard F, Czerwiec T, Henrion G, Segui Y and Loureiro J 2006 *Plasma Chem. Plasma Process.* **26** 251-266
[133] Reuter R, Rügner K, Ellerweg D, de los Arcos T, von Keudell A and Benedikt J 2012 *Plasma Process. Polym.* **9** 1116-1124
[134] Zaera F 2013 *Coord. Chem. Rev.* **257** 3177-3191
[135] Guaitella O, Lazzaroni C, Marinov D and Rousseau A 2010 *Appl. Phys. Lett.* **97** 011502
[136] Ohshima T, Kondo T, Kitajima N and Sato M 2010 *IEEE Trans. Ind. Appl.* **46** 23-28
[137] Thevenet F, Sivachandiran L, Guaitella O, Barakat C and Rousseau A 2014 *J. Phys. D: Appl. Phys.* **47** 224011
[138] Huang H, Xu Y, Feng Q and Leung D Y C 2015 *Catal. Sci. Technol.* **5** 2649-2669
[139] Bourdon A and Bultel A 2008 *J. Thermophys. Heat Trans.* **22** 168-177
[140] Marschall J and MacLean M 2011 *42nd AIAA Thermophys. Conf.* (Reston Virginia: American Institute of Aeronautics and Astronautics)
[141] Arasa C, Gamallo P and Sayós R 2005 *J. Phys. Chem.* B **109** 14954-14964
[142] Rutigliano M, Pieretti M, Cacciatore M, Sanna N and Barone V 2006 *Surf. Sci.* **600** 4239-4246
[143] Meana-Pañeda R, Paukku Y, Duanmu K, Norman P, Schwartzentruber T E and Truhlar D G 2015 *J. Phys. Chem.* C **119** 9287-9301
[144] Graves D B and Brault P 2009 *J. Phys. D: Appl. Phys.* **42** 194011
[145] Despiau-Pujo E, Davydova A, Cunge G, Delfour L, Magaud L and Graves D B 2013 *J. Appl. Phys.* **113** 114302

[146] Neyts E C and Bogaerts A 2014 *J. Phys. D: Appl. Phys.* **47** 224010
[147] Neyts E C and Brault P 2017 *Plasma Process. Polym.* **14** 1600145
[148] Sørensen M R and Voter A F 2000 *J. Chem. Phys.* **112** 9599-9606
[149] Voter A F 1997 *J. Chem. Phys.* **106** 4665-4677
[150] Bal K M and Neyts E C 2015 *J. Chem. Theory Comput.* **11** 4545-4554
[151] Guerra V and Marinov D 2016 *Plasma Sources Sci. Technol.* **25** 045001
[152] Marinov D, Teixeira C and Guerra V 2017 *Plasma Process. Polym.* **14** 1600175
[153] Gillespie D T 1976 *J. Comput. Phys.* **22** 403-434
[154] Gillespie D T 1977 *J. Phys. Chem.* **81** 2340-2361
[155] Reese J S, Raimondeau S and Vlachos D G 2001 *J. Comput. Phys.* **173** 302-321
[156] Kovalev V L, Sazonenko V Yu and Yakunchikov A N 2007 *Mosc. Univ. Mech. Bull.* **62** 53-58
[157] Jansen A P J 2012 *An Introduction to Kinetic Monte Carlo Simulations of Surface Reactions*, vol. 856 (Heidelberg:Springer)
[158] Cuppen H M, Karssemeijer L J and Lamberts T 2013 *Chem. Rev.* **113** 8840-8871
[159] van Kampen N G 1992 *Stochastic Processes in Physics and Chemistry* (Amsterdam: Elsevier Science)
[160] Gillespie D T 1992 *Markov Processes: An Introduction for Physical Scientists* (London: Academic Press Limited)
[161] Bortz A B, Kalos M H and Lebowitz J L 1975 *J. Comput. Phys.* **17** 10-18
[162] Fichthorn K A and Weinberg W H 1991 *J. Chem. Phys.* **95** 1090-1096
[163] Kim Y C and Boudart M 1991 *Langmuir* **7** 2999-3005
[164] Seward W A and Jumper E J 1991 *J. Thermophys. Heat Trans.* **5** 284-291
[165] Gordiets B F and Ferreira C M 1998 *AIAA Journal* **36** 1643-1651
[166] Guerra V 2007 *IEEE Trans. Plasma Sci.* **35** 1397-1412
[167] Lopaev D V, Malykhin E M and Zyryanov S M 2011 *J. Phys. D: Appl. Phys.* **44** 015201
[168] Guerra V, Marinov D, Guaitella O and Rousseau A 2014 *J. Phys. D: Appl. Phys.* **47** 224012
[169] Guaitella O, Hübner M, Welzel S, Marinov D, Röpcke J and Rousseau A 2010 *Plasma Sources Sci. Technol.* **19** 45026
[170] Marinov D, Guaitella O, Booth J P and Rousseau A 2013 *J. Phys. D: Appl. Phys.* **46** 032001

List of symbols, physical constants and acronyms

Table 1. List of symbols.

Symbol	Unit	Description
$F_\alpha(\vec{r},\vec{v}_\alpha,t)$	$\mathrm{m}^{-6}\ \mathrm{s}^3$	α-particle distribution function ($\alpha = e, i$)
$f^0(u)$	$\mathrm{eV}^{-3/2}$	electron energy distribution function
m_k	kg	mass of species k ($k = \alpha$ for charge particles; $k = o$ for neutrals)
M	kg	gas atomic / molecular mass
n_k	m^{-3}	number density of species k
n_0	m^{-3}	ground-state density of the neutral gas
T_k	K	temperature of species k
T_g	K	gas temperature
p	Pa	gas pressure
ε_k	eV	mean energy of species k
$\vec{X}_\alpha$	N	external force acting on the charged particles α
$\vec{E} = \vec{E}_{\mathrm{ext}} + \vec{E}_s$	$\mathrm{V\ m}^{-1}$	total (external + space-charge) electric field
E/n_0	$\mathrm{V\ m}^2$	reduced electric field
σ_{ion}	m^2	electron-neutral ionisation cross section
σ_m	m^2	electron-neutral total momentum-transfer cross section
$\sigma_{m,\mathrm{el}}$	m^2	electron-neutral elastic momentum-transfer cross section
σ_{ij}	m^2	electron-neutral scattering cross section for $i \to j$ transition
u_{ij}	eV	excitation energy for $i \to j$ transition
δ_i		fractional population density of state i
ν_{ee}	s^{-1}	electron-electron collision frequency
$\langle\nu_{m_k}\rangle \equiv \nu_k$	s^{-1}	average momentum-transfer frequency for collisions between k-species and neutrals
$\langle\nu_{\mathrm{ion}}\rangle$	s^{-1}	average ionisation frequency
S_k	$\mathrm{cm}^{-3}\mathrm{s}^{-1}$	net production rate (source term) for species k
$\vec{v}_{d_k}$	$\mathrm{cm\ s}^{-1}$	drift velocity for species k
$\vec{\Gamma}_k \equiv n_k\vec{v}_{d_k}$	$\mathrm{cm}^{-2}\mathrm{s}^{-1}$	particle flux for species k
$\vec{\Gamma}_{\varepsilon_k}$	$\mathrm{eV\ cm}^{-2}\mathrm{s}^{-1}$	energy flux for species k
$\mu_k n_0$	$\mathrm{V}^{-1}\mathrm{m}^{-1}\mathrm{s}^{-1}$	reduced mobility of species k
$D_k n_0$	$\mathrm{m}^{-1}\mathrm{s}^{-1}$	reduced diffusion coefficient of species k
σ_α	$\Omega^{-1}\mathrm{m}^{-1}$	conductivity of species α
$\mu_{\varepsilon_k} n_0$	$\mathrm{m}^{-1}\mathrm{s}^{-1}$	reduced mobility for the energy of species k
$D_{\varepsilon_k} n_0$	$\mathrm{eV\ m}^{-1}\mathrm{s}^{-1}$	reduced diffusion coefficient for the energy of species k
α	m^{-1}	ionisation Townsend coefficient
α/n_0	m^2	reduced ionisation Townsend coefficient
λ_k	m	mean-free-path of species k
λ_D	m	Debye length
Λ	m	characteristic diffusion length
k_j	$\mathrm{m}^3\mathrm{s}^{-1}$	rate coefficient for chemical reaction j

Table 2. List of physical constants.

Symbol	Description
k_B	Boltzmann constant
e	electron charge
ε_0	vacuum permittivity

Table 3. List of acronyms.

Acronym	Meaning
BKL	Bortz-Kalos-Lebowitz
CCRF	capacitively coupled radio-frequency
DBD	dielectric barrier discharge
DC	direct current
DD	deterministic description
EBE	electron Boltzmann equation
EEDF	electron energy distribution function
KMC	Kinetic Monte Carlo
LEA	local mean energy approximation
LFA	local field approximation
LTP	low-temperature plasma
MC	Monte Carlo
PIC	particle-in-cell
PIC-MCC	particle-in-cell with Monte-Carlo collisions
VDF	vibrational distribution function